



Immunoresponsive microbiota-gut-on-chip reproduces barrier dysfunction, stromal reshaping and probiotics translocation under inflammation

Vincenza De Gregorio ^{a,b}, Cinzia Sgambato ^b, Francesco Urciuolo ^{a,c}, Raffaele Vecchione ^b, Paolo Antonio Netti ^{a,b,c}, Giorgia Imparato ^{b,*}

^a Interdisciplinary Research Centre on Biomaterials (CRIB), University of Naples Federico II, Naples, Italy

^b Center for Advanced Biomaterials for HealthCare@CRIB, Istituto Italiano di Tecnologia, Naples, Italy

^c Department of Chemical, Materials and Industrial Production Engineering (DICMAPI) University of Naples Federico II, Naples, Italy



ARTICLE INFO

Keywords:

Human microbiota-intestine axis on chip
Mucosal immunity
Oxygen gradient
Extracellular microenvironment
Intestinal microbiota
Inflammatory bowel disease

ABSTRACT

Here, we propose an immune-responsive human Microbiota-Intestine axis on-chip as a platform able to reproduce the architecture and vertical topography of the microbiota with a complex extracellular microenvironment consisting of a responsive extra cellular matrix (ECM) and a plethora of immune-modulatory mediators released from different cell populations such as epithelial, stromal, blood and microbial species in homeostatic and inflamed conditions. Firstly, we developed a three-dimensional human intestine model (3D-hI), represented by an instructive and histologically competent ECM and a well-differentiated epithelium with mucus-covered microvilli. Then, we replicated the microenvironmental anaerobic condition of human intestinal lumen by fabricating a custom-made microbiota chamber (M_C) on the apical side of the Microbiota-human Intestine on chip (MiHI-oC), establishing the physiological oxygen gradient occurring along the thickness of human small intestine from the serosal to the luminal side. The complexity of the intestinal extracellular microenvironment was improved by integrating cells populations that are directly involved in the inflammatory response such as peripheral blood mononuclear cells (PBMCs) and two species of the intestinal commensal microbiota (*Lactobacillus rhamnosus* and *Bifidobacterium longum*). We found that lipopolysaccharide (LPS)-induced inflammation elicits microbiota's geographical change and induce *Bifidobacterium longum* iper-proliferation, highlighting a role of such probiotic in anti-inflammatory process. Moreover, we proved, for the first time, the indirect role of the microbiota on stromal reshaping in immune-responsive MiHI-oC in terms of collagen fibers orientation and ECM remodeling, and demonstrated the role of microbiota in alleviating gastrointestinal, immunological and infectious diseases by analyzing the release of key immune-mediators after inflammatory stimulus (reactive oxygen species (ROS), pro- and anti-inflammatory cytokines).

1. Introduction

The development of novel and reliable human intestinal *in vitro* models able to replicate the crosstalk between living microbial components, intestinal mucosa, and immune system, is a fundamental technological tool to aid researchers in elucidating the role of microbiota in maintaining intestinal health and immune regulation [1]. Until recently, the gut-microbiome crosstalk has been mainly investigated by performing omics analyses on the samples collected *in vivo*, allowing researchers to characterize the composition and functionality of complex microbial communities and identifying microbes, or microbial

metabolites, which correlate with a disease state (e.g. inflammatory bowel disease, IBD) at a single time point (cross-sectional studies) underestimating the continuous and direct interaction between intestinal mucosa and microbiota in sustaining intestinal tissue homeostasis [2]. *In vivo* animal studies have been also performed, but present limited transferability to the human situation, due to the different composition of the microbiota, as well as immune system [1]. On the other side, well-established cell lines, such as Caco-2 cells, cultured as monolayers on extracellular matrix-coated standard plastic dishes or transwell inserts, are frequently exploited in tissue engineering to study human intestinal epithelial cells *in vitro*. Although these two-dimensional (2D)

* Corresponding author. Center for Advanced Biomaterials for HealthCare@CRIB Istituto Italiano di Tecnologia, Largo Barsanti e Matteucci n. 53, 80125, Napoli, Italy.

E-mail address: giorgia.imparato@iit.it (G. Imparato).

culture techniques have elucidated numerous aspects of intestinal epithelial cell biology, it should be noted that they do not recreate typical micro-anatomical structures of the human intestine including the physiological microbiota stratification existing in the intestinal lumen [3]. Indeed, the microbiota is biogeographically stratified within the gastrointestinal tract on different spatial scales and axes and its viability is strictly dependent on the oxygen gradient that increases precipitously along the serosal-luminal transversal section [4]. To fully understand the functionality of the intestinal microbiota, greater attention must be paid to the microhabitats within the intestinal ecosystem and the spatial relationships among microorganisms and between microorganisms and the host. Moving inward along the crypt-villus axis the surface of the macrovilli and crypts is colonized by adherent species [4] and the epithelium colonized by obligate anaerobic bacteria completely embedded within the mucus at the lumen side [5]. This bacterial stratification is strictly related to the intraluminal oxygen gradient and has been extensively shown to have profound effects on population dynamics and ecosystems that in turn affect the intestinal tissue functionality [6]. Unfortunately, gut microbiome spatial organization is destroyed when DNA is extracted from human/mouse intestinal cuts or stool samples to perform genomic analysis and can be investigated only in intestinal *in vitro* model in which the direct interaction among human gut microbiota, epithelial cells, and mucus is replicated allowing the mimicry of a physiological crosstalk. Recently, great attention has been given to the integration of tissue engineering approaches with microfluidics techniques to mimic *in vitro* the paracrine and endocrine cross-talk between gut microbiota and intestinal mucosa. Some models have been proposed in which intestinal gut microbiota and intestinal mucosa are separated in different modules [7] or by porous membranes coated with synthetic mucus [8] or posed in direct contact in double layer model (epithelial, endothelial cells) introducing the mechanical stretch to mimic the peristalsis motion [9]. However, all these models, are still based on intestinal epithelial cells grown on synthetic substrates non-considering the key role of the lamina propria, in terms of molecular composition and mechanical properties, in affecting epithelium morphogenesis, immunological response, microbial behavior as well as disease progression [10,11]. We have previously demonstrated the capability of recapitulating *in vitro* the intestinal pathophysiological environment including the morphology and macromolecular composition of the lamina propria and demonstrated its role in maintaining undifferentiated phenotype of proliferative cells in the basal crypts guiding epithelium morphogenesis, sustaining stemness of germinal layer and contributing in innate immune response under inflammatory stimulus [12]. This was in agreement with other studies that highlight the role of the lamina propria in dictating intestinal cells behavior demonstrating that the ECM of lamina propria provides the supportive biomechanical properties for epithelial and mesenchymal cells along the crypt-villus axis [13]. Here, we developed an immune-responsive Microbiota-human Intestine axis on chip in which microbiota species, vertically stratified, are in direct contact with a complex intestinal environment consisting of a responsive three-dimensional (3D) basal lamina, a fully differentiated epithelium and circulating PBMCs. A custom-made M_C allows establishing the target luminal-serosal oxygen gradient, as calculated theoretically and confirmed experimentally. This gradient is pivotal to sustain the viability, growth and physiological vertical distribution of microbiota. We proved the role of microbiota in preventing epithelial injury and, for the first time, we demonstrated the indirect role of the microbiota on stromal reshaping in terms of collagen fibers orientation, ECM remodeling and ROS production. We also demonstrated that an imbalance in mucus-embedded-bacteria in inflamed MihI-oC changes the immune response by analyzing the secretome - collecting luminal and serosal eluates - so elucidating the role of microbiota in alleviating gastrointestinal, immunological and infectious diseases. To conclude the microbiota as well as PBMCs supplementation determined a more faithful recapitulation of the mucosal-associated microbiota-cell interactions into the complex

microenvironment in both physiological and pathological conditions.

2. Materials and methods

2.1. Cells and microbial strains culture conditions

Human colonic epithelial cell lines (Caco-2) were purchased by American Type Culture Collection (ATCC) and cultured in High-glucose DMEM (Hg-DMEM, GIBCO) supplemented with 10% of fetal bovine serum (FBS), 2 mM L-glutamine, and 100 U mL⁻¹ penicillin and streptomycin (Sigma Aldrich, St. Louis, MO, USA) and grown at 37 °C in a 5% CO₂ humidified incubator. Human intestinal subepithelial myofibroblasts (hiSEMfs) from human ileal mucosa obtained by endoscopic duodenal biopsies from adult subjects after informed consent were kindly donated by European Laboratory for the Investigation of Food-Induced Diseases - University of Naples Federico II [14] and cultured in DMEM supplemented with 10% heat-inactivated FBS, 2 mM L-glutamine, and 100 U mL⁻¹ penicillin and streptomycin (Sigma Aldrich, St. Louis, MO, USA). Cells at the passages 6–8 were used for the experimental phase. PBMCs were isolated by using buffy coat separation from whole blood; 30 mL of peripheral human blood taken from healthy donors were collected, after informed consent, into BD Vacutainer™ Plastic Blood Collection Tubes with K2EDTA to avoid coagulation. The whole blood volume was diluted 1:1 with phosphate-buffered saline (PBS, Sigma Aldrich, St. Louis, MO, USA) and put on an equal volume of a density gradient media (Ficoll, Sigma Aldrich, St. Louis, MO, USA) in standard 50 mL plastic tubes. The samples were centrifuged at 250 g × 30 min without using the machine brake. Subsequently, the resulting PBMC ring was collected using a standard glass Pasteur pipette and washed twice with Red blood cell lysis buffer to exclude the erythrocyte contaminations of the sample. Afterward, PBMC were concentrated at 10⁶ cells/mL and flowed into the S_C of the microfluidic device. Two strains of probiotic bacteria were obtained in commercial lyophilized form, namely *Lactobacillus rhamnosus* (*L. rhamnosus*) GG strain (ATCC 53103) and *Bifidobacterium longum* (*B. longum*) (*subspp infantis*) (ATCC 15697). The first one was grown 18–24 h in static de Man-Rogosa-Sharpe broth (MRS, Oxoid, Basingstoke Hampshire, United Kingdom) in microaerophilic condition based on an atmosphere of 10% H₂, 10% CO₂ (Concept plus anaerobic workstation (AW), Ruskinn technology limited) at 37 °C, while the second one was cultured in M151 medium (Oxoid, Basingstoke Hampshire, United Kingdom) for 24–48 h in an anaerobic incubator with an anaerobic gas mixture 10% H₂, 10% CO₂, and 80% N₂ or in 100% N₂ (Concept plus AW, Ruskinn technology limited, Rome, Italy). For each bacterial strain, five colonies were collected, inoculated into the previously degased selective broth media, and incubated at 37 °C for 18–24 h in microaerophilic (*L. rhamnosus*) or in anaerobic conditions (*B. longum*). For the experimental phase, aliquots (50 µl) of the bacterial suspensions were refreshed into 20 mL of fresh growth media and cultured for 2 h at the optimal culture conditions. The optical density was read at 600 nm (OD600) by turbidimetric analysis (BioPhotometer Eppendorf, Milan, Italy) and bacterial suspensions at the exponential phase were selected.

2.2. Organotypic 3D human intestine (3D-hI) model production

Gelatine porous microscaffolds having a diameter of 75–150 µm, stabilized by 4% of glyceraldehyde were fabricated by means of a modified double emulsion technique (O/W/O) as previously reported [14]. Briefly, gelatine (type B, Sigma Aldrich, St. Louis, MO, USA, Bloom 225, Mw 176,654 Da) was dissolved into 10 mL of water containing TWEEN 85 (6% w/v) (Sigma Aldrich, St. Louis, MO, USA) at 60 °C. A mixture of toluene and SPAN 85 (3% w/v; Sigma Aldrich) was constantly added to the aqueous gelatin solution (8% w/v; Sigma Aldrich, St. Louis, MO, USA) to obtain primary oil in water emulsion. Microscaffolds containing droplets of toluene were produced through the addition of excess toluene (30 mL) and then cooled at 4 °C.

Subsequently, in order to extract toluene and stabilize the micro-scaffolds, 20 mL of ethanol were added, and the newly produced microspheres were filtered, washed with acetone, and dried at room temperature. To produce the human intestine microtissue, a suspension containing hISEMFs ($1 \cdot 10^5$ hISEMFs/mL) and 2 mg/mL of microscaffold (10 cells per bead) was transferred to a spinner flask bioreactor (250 mL, CELLSPIIN, Integra Biosciences, Corston - UK) for at least 10 days. The culture suspension was stirred intermittently at 10 rpm (5 min stirring and 40 min in static condition) for the first day in order to promote cell adhesion; then the stirring velocity was increased to 20 rpm for the further 10 days. All cultures were maintained at 37 °C in a humidified 5% CO₂ incubator. Three times per week the media was replaced and 2-O-alpha-D-Glucopyranosyl-L-ascorbic Acid 0.5 mM (TCI Europe) was added. Then, the human intestine microtissue were harvested from spinner cultures and transferred into a suitably designed assembling chamber, which contains a silicon mold with disc-shaped spaces (1 mm in thickness, 10 mm in diameter), where the human intestine microtissue biological assembling takes place. Stainless steel rigid grids are posed directly on both sides of the system. Then, two polytetrafluoroethylene rings are located on the grids on both system sides and are fastened to each other by means of stainless steel screws, which close the system to ensure that the human intestine microtissue are retained. The system is autoclavable in each part. Additionally, after accommodating the assembling chamber, the spinner flask has been set to operate at 60 rpm to ensure the continuous media stirring and the medium was changed three times per week. After 3 weeks of culture, the assembling chamber was opened and the 3D Intestinal stroma samples were collected, rinsed twice with PBS solution, and accommodated in 12-well plate transwell with permeable polycarbonate membrane inserts (diameter, 12 mm; Corning®, USA) allowing drying for 5 min under laminar flow. Subsequently, 50 µL of the Caco-2 suspension was seeded to the center of each 3D intestinal stroma, corresponding to 2×10^5 cells for sample to obtain the 3D human intestine model (3D-hI). The transwell insert was incubated for at least 2 h in an incubator at 37 °C with 5% CO₂ to allow Caco-2 adhesion onto the 3D intestinal stroma surface. Then, the complete medium (200 µL) was added in the apical side of the transwell insert and the basolateral side was filled with 600 µL of DMEM, to achieve a submerged culture promoting Caco-2 polarization. The submerged culture lasted approximately 7 d. Then, an optimized air-liquid interface culture lasting 2 weeks took place in order to induce the epithelial tissues to polarize and differentiate. The culture medium was replaced on the first day and three times for week until the end of the experiments. At the end of the air-liquid interface culture, 3D-hI was moved from the 12-well plate transwell to the Snapwell® (polycarbonate insert diameter 13 mm, pore size 12.0 µm, Merk Millipore, Darmstadt, Germany) of the Mihi-oC.

2.3. Microbiota human intestine on chip (Mihi-oC) design and assembly

2.3.1. Human intestine on chip (hi-oC)

The microfluidic device for hosting 3D-hI was fabricated by using replica molding of polydimethylsiloxane (PDMS; Sylgard 184; Mascherpa) from a poly (methyl methacrylate) (PMMA, Goodfellow) master as reported in detail in the Supplementary Figure. S1. The PMMA master was designed by AutoCAD and carved with Micromilling machine (Minitech CNC Mini-Mill). The resulting PDMS replica presents a central microchannel (1 mm wide × 5 mm long × 1 mm high) with an opened central chamber (13 mm diameter × 5 mm high) in which the Snapwell® insert was aseptically placed separating the intestinal compartment (I_C) such as the apical-luminal side of the hi-oC from the Serosal compartment (S_C), such as the basal-serosal side of the hi-oC. The ratio of PDMS pre-polymer and curing agent was 10:1 (w/w); then, the mixture was degassed under vacuum for 20 min to remove air bubbles and poured on the PMMA master. The PDMS slab was left at 80 °C for 60 min, then peeled off from the master. Inlet and outlet holes of the S_C were punched with a 1 mm biopsy punch (from Cantabria Labs,

DIFA COOPER S. p.A, Milan - Italy). The micro-channel was closed by bonding the PDMS device to a glass coverslip (24 mm wide × 60 mm long) by oxygen plasma treatment for 1 min at 50 W in an oxygen plasma oven (Plasma Femto, Diener, Diener electronic GmbH, Ebhausen - Germany). Subsequently, the whole setup was left at 80 °C overnight to achieve irreversible bonding of the PDMS and the glass.

2.3.2. Microbiota chamber (M_C) fabrication

The M_C was designed to provide the hi-oC with the microenvironmental anaerobic conditions necessary for bacterial growth. The M_C consists of a PMMA lid placed on the I_C (Supplementary Figure. S2). PMMA was chosen since it possesses a very low oxygen diffusion coefficient (2.7×10^{-8} cm² s⁻¹) compared to PDMS (3.25×10^{-5} cm² s⁻¹), or polycarbonate (1×10^{-5} cm² s⁻¹). To establish the geometry of the M_C to provide the optimal flow of N₂ into the luminal compartment of I_C, different dimensions were explored and tested by modulating the N₂ flow rate at the inlet of the M_C. In the final and optimal configuration, M_C presents a cylindrical geometry with a diameter of 15 mm and an height of 25 mm and it is provided with an inlet for N₂ entry and an outlet for exit. The M_C is opportunely accommodated on the hi-oC thanks to the presence of a circular track (Figure S2, E1) around the I_C to produce the Mihi-oC as described in detail in the Supplementary materials (Figure S2). Then, M_C was connected to a pressure pump (Dolomite) that flush the N₂ inside the chamber through the inlet, to completely eject the oxygen. The N₂ flow rate was optimized by using COMSOL simulation.

2.3.3. Assessment of functionality of M_C by evaluating bacterial viability and growth

2.3.3.1. Bacterial total and viable count. To assess the ability of M_C to correctly replicate the microenvironmental anaerobic conditions necessary for bacterial strains culture, the viability of the single bacteria strain was monitored by culturing it in i) microaerophilic conditions in the anaerobic workstation (micro-AW), ii) anaerobic conditions in the anaerobic workstation (ana-AW) or iii) hypoxic environment generated into the M_C of the Mihi-oC. A solution of bovine type I collagen (Sigma Aldrich, St. Louis, MO, USA) at a concentration of 5 mg/mL and neutralized by dropwise addition of 0.1 NaOH was prepared and added into a Snapwell® insert. After placing Snapwell® in an incubator at 37 °C for 45 min the polymerization of the collagen occurred resulting in a disc-shaped gel that covered the pores and avoided the bacterial crossing through the porous membranes into the S_C. Then, 500 µL of refreshed suspension of each bacterial strain (OD 600 = 0.5 nm), grown in selective broth media, was placed on the collagen disc-shaped gel in the Snapwell® insert of the Mihi-oC. A thin PDMS layer (100 µm thickness) fabricated by PDMS precursor spin coating (1000 rpm × 30 s) was used to cover the Snapwell® and then the Mihi-oC was placed in the ana- or micro-AW or connected to a pressure pump to allow the nitrogen flow into the M_C. Triplicate was performed for each condition. For all the configurations the S_C of Mihi-oC was connected to a syringe pump (Ismatec) and a specific flow rate (30 µL/min) was imposed. To determine the total counts of each bacterial suspension, aliquots of 10 µL were collected every 15 min from the apical side of Snapwell® insert over a 32–36 h period, leading to volume of 1 mL, and the optical density at 600 nm (OD600) was read by turbidimetric analysis (BioPhotometer Eppendorf, Milan, Italy). Meantime, to define the total number of surviving bacteria, a viable count assay for each culture condition was also performed. The 10-fold serial dilutions of the bacterial suspension were prepared in PBS and 3 drops of 10 µL from each dilution were plated on selective solid media (MRS or CM151) and incubated at 37 °C for 24–48 h in above-mentioned hypoxic conditions. After the incubation time, the colonies that grew on these plates were counted and the colony-forming units CFU/mL were calculated to quantify bacteria surviving. At last, turbidimetric measurement was correlated with growth curves of viable

bacteria. Each test was performed in triplicate and repeated at least three times.

2.3.3.2. Bacterial live/dead assay. The total count of viable/not-viable bacteria was assessed by using the Live/Dead BacLight Bacterial Viability Stain Kit (Molecular Probes, Eugene, OR). First of all, the best concentration of the viability kit stain mixture (SYTO9 and propidium iodide -PI-) was selected, which allowed us to distinguish the live bacterial cells from dead (SYTO9: PI, 1:2 v/v). Briefly, freshly grown bacteria suspensions (*L. rhamnosus* or *B. longum*) were opportunely diluted and harvested by centrifugation (3200×g, for 15 min) and washed three times with NaCl 0.85% solution. Then, 3 µL of a mixture of SYTO9 and PI (1:2) were diluted in 0.5 mL of bacterial suspension directly on the apical side of the Snapwell® insert and incubated in darkness for 15 min at room temperature according to the manufacturer's instructions. Non-viable bacteria were prepared by 95% ethanol treatment of the bacteria for 30 min. The bacteria were washed twice with NaCl 0.85% after the treatments and examined under Leica confocal microscope (Confocal Leica TCS SP5 II femtosecond laser scanning system, Leica). Filters were set to 493–522 nm for SYTO9 and 618–676 nm for PI. CLSM images were obtained with 40× objective (optical zoom 1.5). Each sample was scanned at randomly selected areas as a series of vertical optical sections, each one 0.50 µm thick. Quantitative analyses of each bacterial strain were carried out by analyzing the digital images of live (green) and dead (red) bacteria with Image J software. Each image was divided in ROIs with comparable areas, and the thresholding was performed. The fluorescence intensity per unit area was measured and calculated as percentage of viable cells.

2.3.4. MihI-oC operative set up with 3D-hI and microbiota

Before tissue culture, the devices, the tubes, and the connectors were sterilized by autoclaving. 2-Stop Tygon sterilized tubes were inserted into the inlet and outlet channel of the MihI-oC using sterilized male luer lock connectors (Harvard Apparatus, Massachusetts, USA). After accommodating the 3D-hI into the I_C a sealing silicon ring (Figure S2 B and C) was placed on the 3D-hI to co-culture the bacterial strains on the luminal side of the 3D-hI, avoiding basal contamination. The sealing ring was made-up by punching 1 mm thick silicon layer, first with a 6.5 mm puncher (for the inner hole) and then with a 13 mm puncher (for the outer hole) and sterilized under UV light. The exponentially growing bacteria (*L. rhamnosus* and *B. longum* at a ratio 1:1) were loaded on the luminal side of the 3D-hI model directly on-chip (the co-culture of microbial strains will report as microbiota from now on). Briefly, overnight culture of each strain (*L. rhamnosus* and *B. longum*) was refreshed for 4 h in the selected media and the turbidity was adjusted to obtain the optimal bacteria concentration (OD 0.5–10⁶ CFU/mL) to add in a 1:1 ratio onto the apical surface of 3D-hI in the I_C of the MihI-oC. Then, 500 µL of DMEM-dispersed microbiota was added onto the apical side of the 3D-hI. For preventing the bacterial contaminations and to ensure the gas exchange with M_C but avoiding the evaporation issue of the medium, the I_C was closed laying a thin layer of PDMS (100 µm thickness) fabricated as reported above. The micro-channels of the S_C were connected to a syringe pump (Ismatec) and the flow rate of culture medium was set at 30 µL/min after performing COMSOL simulation (Supplementary Figure. S3 and S4). Meanwhile the M_C was connected to a pressure pump to establish hypoxic environmental condition. Since the N₂ comes out in the M_C at 24 °C temperature, whereas the temperature for the optimal growth of the microbiota is 37 °C, a pre-warmed microbiota suspension was loaded into the apical side of MihI-oC into the anaerobic bacterial glove box, then the entire setup was transferred into a cell incubator and the temperature was monitored with a hand-made Arduino set-up to evaluate the time required from the system to reach the optimal microbiota growth temperature (37 °C) (Supplementary Figure. S5). Once obtained the anoxic condition, the N₂ flux was maintained at 5 µL/min with a very low Reynolds number (4·10⁻⁶) to ensure laminar flow

on the liquid interface which hosts the microbial species into the I_C, obtaining the complete MihI-oC set up. Comsol Multiphysics was used to simulate the oxygen concentration in a given point of the M_C at various N₂ flow rates flushed inside the M_C by a pressure pump, in order to determine the amount of time necessary to eject free oxygen outside the M_C to produce an anoxic environment as reported in the paragraph below. The MihI-oC operated in the incubator for 16 h allowing the co-culture of 3D-hI and microbiota. At the end of the 16 h the co-culture of 3D-hI and microbiota (as well as the 3D-hI alone as control) were collected and processed for histological analysis (Hematoxylin and Eosin (H&E), Alcian blue staining), immunofluorescent staining, and ultrastructural analysis.

2.3.5. Computational model of MihI-oC

The oxygen gradient and the nutrient supply velocity were evaluated by using commercial CFD COMSOL Multiphysics vers. 5.0. CFD analyses were performed dividing the entire device into two different domains: a fluid domain, which identified the region filled with culture medium, and a tissue domain, which identified the region filled with the intestine sample. Simulations within the fluid domain were performed by using the steady state Navier-Stokes equation Eq. (1). No slip boundary conditions were set on the walls, and the fluid was considered to have the same physical characteristics as water. A specific laminar flow was set at the inlet and reference pressure was set at the outlet (p_{ref} = 1atm):

$$\rho(v_1 \cdot \nabla)v_1 = \nabla \cdot [-pI + \mu(\nabla v_1 + (\nabla v_1)^T)] + F \quad (1)$$

$$\rho(v_1 \cdot \nabla) = 0$$

Where μ is the dynamic viscosity, v_1 is the fluid velocity, p is the hydrostatic pressure, and ρ is the fluid density. Brinkman equation Eq. (2) was used to describe the flow through a porous medium:

$$\left(\frac{\mu}{k}\right)v_1 = \nabla \left(-pI + \left(\frac{1}{\varepsilon}\right)(\mu(\nabla v_1 + (\nabla v_1)^T)) \right) - \left(\frac{(2\mu)}{3} - k_{dv}\right)(\nabla \cdot v_1)^l \quad (2)$$

$$\rho(v_1 \cdot \nabla) = 0$$

Where k is the hydraulic permeability, μ is the viscosity of the tissue, p is the pressure, ε is the porosity of the material, k_{dv} is the dynamic permeability. The oxygen concentration within the system was calculated by means of the following mass balance equation Eq. (3):

$$D\nabla^2 C - \nabla(Cv_1) = -R \quad (3)$$

Where C is the oxygen concentration, v_1 is the fluid velocity field, and D is the diffusion coefficient of the oxygen. R is the volumetric oxygen consumption rate expressed by the Michelis-Menten law, according to the following equation Eq. (4):

$$R = \rho \frac{v_{max,1}c}{k_m + c} \quad (4)$$

Where $v_{max,1}$ is the maximum oxygen consumption rate, k_m is the concentration at which the oxygen consumption rate is half of $v_{max,1}$ and ρ is the cell density in the perfusion chamber obtained by taking into account the number of cells present in the Intestine. R was set to 0 in the fluid domain, as cells are present only in the tissue domain. To model the N₂ flow and O₂ transport within the M_C we used a code implemented in COMSOL “Transport of diluted species for compressible fluid with a low Mach”. No slip boundary conditions were set on the walls, and the fluid was considered to have the physical characteristics of nitrogen.

2.3.6. On-line oxygen concentration measurement

During the culture, the oxygen consumption profile inside the M_C was measured by using an optical detector (OXY-4 PreSens) located in

the center of the M_C wall on the opposite side of N_2 flow inlet for 30 min by flowing at a constant rate (200 $\mu\text{L}/\text{min}$) (Supplementary results Figure S2E and F). The measurement was also performed by switching the N_2 flow from 200 $\mu\text{L}/\text{min}$ to 5 $\mu\text{L}/\text{min}$ for 800 min (Supplementary Figure S6).

2.4. Development of immunocompetent Mihi-oC under inflammatory stimulus

To simulate an inflammatory stimulus, the Mihi-oC was treated for 6 h with high concentration (15 $\mu\text{g}/\text{mL}$) of lipopolysaccharides from *Escherichia coli* (LPS; Sigma Aldrich, St. Louis, MO, USA) on the apical side. The *Escherichia coli* working solution was prepared in 2% FBS-supplemented-DMEM from 1 mg/mL (stock solution). The Mihi-oC was cultured overnight in DMEM with FBS reduced from 10% to 2%. Meantime, to produce the immune-competent Mihi-oC, freshly isolated human PBMC were flowed at a concentration of $10^6/\text{mL}$ by means of a syringe pump operating at 30 $\mu\text{L}/\text{min}$. A reservoir was connected to the S_C of the Mihi-oC to collect the metabolites. The LPS treatment last 6 h. For each experiment, three parallel devices were used and different combination with or without LPS and PBMC were explored: Inflamed human intestine on-chip ($hI\text{-oC}_{LPS}$), Inflamed Microbiota human Intestine on chip ($Mihi\text{-oC}_{LPS}$), Immune-responsive human intestine on chip ($hI\text{-oC}_{PBMC}$), Immune-responsive Microbiota human Intestine on chip ($Mihi\text{-oC}_{PBMC}$), Inflamed Immune-responsive human intestine on chip ($hI\text{-oC}_{LPS} + PBMC$), Inflamed Immune-responsive Microbiota human Intestine on chip ($Mihi\text{-oC}_{LPS} + PBMC$). At the end of the 6 h all tissue samples were collected and processed for immune-histotypical and molecular characterizations. In addition, the media collected were analyzed for metabolites produced on both the apical and basal side of the I_C (ELISA assay). Moreover, ultrastructural SEM analysis was performed as reported above with slight protocol modifications' in the fixation and dehydration procedures. Briefly, the samples were fixed with 2.5% (v/v) glutaraldehyde and by adding 1% of alcian blue for 2 h at room temperature and were dehydrated at a gradually increasing percentage of ethanol (10%, 15%, 20%, etc.) in order to preserve the bacteria adhered on the surface and the mucus.

2.5. Ultrastructural and morphological characterization of microbiota

For SEM analysis, the bacterial suspension of each strain, collected from the apical side of I_C of Mihi-oC, was seeded on 0.1% gelatin-coated glass accommodated into Petri dish of 3.5 cm^2 and fixed with 2.5% (v/v) glutaraldehyde for 2 h at room temperature and washed twice in 100 mM cacodylate buffer pH 7.2, for 10 min at room temperature. A second fixation in 1% (w/v) osmium tetroxide, buffered in 100 mM cacodylate pH 7.2, was done overnight at 4 °C. Dehydration was carried out in a graded ethanol series (30, 50, 70, 90 and 100%) for 10 min each and samples were then treated with liquid carbon dioxide using a Critical Point Dryer (Emitech K850). Dried samples were mounted onto metal stubs, sputter coated with gold-palladium at 10 mA. Coated samples were then, examined by scanning electron microscopy (SEM) (Leica S400). For morphological characterization the bacterial suspensions were collected from the I_C of Mihi-oC by removing the M_C and then loaded on 0.1% gelatin-coated glass, heat-fixed and let it dry for 1 h and stained by using standard protocol as described by the manufacturer (Gram staining, Biooptica).

2.6. Histotypical tissue characterization

For histological characterization and confocal acquisitions, the samples were appropriately processed without removing the silicon ring into hI - or Mihi-oC and gently fixed by adding to the Snapwell wall drop by drop a solution of 10% (v/v) neutral buffered formalin for 1 h or fresh 4% (w/v) formaldehyde solution, respectively. Then, the samples were harvested from Snapwell and weakly rinsed in PBS. Subsequently, the

samples were carefully dehydrated in a gradual incremental series of alcohol (30, 50, 70, 80, 90 and 100% twice, each step 30 min at RT). In particular, the dehydration process took place very gradually to avoid the detachment of the mucus and/or microbiota from the samples. For which, at each step, half of alcohol was removed, and the higher graded alcohol was added, avoiding drying of the sample. Following dehydration, the 3D tissues was incubated with xylene to clear any remaining ethanol (30 min twice) and the orientated samples were embedded in paraffin at 60 °C and subsequently allowed to harden overnight. The paraffin-embedded cooled samples were subsequently cut with a sharp blade into ultra-thin slices using a microtome (5 μm thickness) (MICROM HM355S Bioptica, Milan - Italy). Then, the sections are dried onto on a heating plate and stored at room temperature. Tissue sections from 3D-hI with or without microbiota were stained with H&E or Alcian blue and the coverslips were mounted with Histomount mounting solution (Bioptica, Milan - Italy). For immunofluorescence analyses the glasses were mounted with glycerol 50% (v/v) in water. For quantitative evaluation, the intestinal epithelial thickness was measured by using Image J software quantifying H&E stained sections with line selection tool randomly posed perpendicular to the stromal compartment per each field. The measurement scale was calibrated using the micron scale of each image. To quantify the mucus secretion, samples were processed by using color deconvolution plugin of Image J software. Automatic thresholding was applied and blue staining, indicating mucus secretion, was separated from other colors. Further, the mucus deposition was quantified as the mean percentage of blue stained region. Ten sections were used and at least five different fields were randomly examined in each section for histochemical characterization.

2.7. Molecular analyses: bacterial DNA isolation and reverse transcription-polymerase chain reaction analysis

For the biomolecular extractions, the microbial cells were disrupted and withdrawn from the Mihi-oC at the end of the culture time using a plastic scrapper or tip and placed in a 0.9% (w/v) NaCl solution. This solution was then collected in a sample tube and centrifuged at 4000 r.p.m. for 10 min at 4 °C to pellet the bacteria. The supernatant was discarded and the bacterial pellet was frozen. The bacterial DNA was extracted using the QIAamp® DNA Stool Mini Kit (QIAGEN) following the manufacturer's protocol with slight modification and then immediately stored at -20 °C. Specific primers were used to quantify the relative abundances of the two bacterial species by amplifying the following primers: BifidF 5' - CTC-CTG-GAA-ACG-GGT-GG - 3' and BifidR 5'- GGT-GTT-CTT-CCC-GAT-ATC-TAC-A - 3' for *B. longum*, and W3_For 5' - TGC-ATC-TTG-ATT-TAA-TTT-TG - 3' and Y2_Rev 5' - CCC-ACT-GCT-GCC-TCC-CGT-AGG-AGT - 3' for *L. rhamnosus*. Resultant sequences were analyzed using the spectrophotometer and gel images were performed by densitometry using Image J software. The relative abundances of *L. rhamnosus* and *B. longum* was expressed in percentage; the ribosomal DNA (rDNA) level was calculated as ng/mL and total microbial DNA amount was reported as microbiota biomass and normalized to 100%. For molecular analysis of $hI\text{-oC}_{LPS}$ and $Mihi\text{-oC}_{LPS}$ samples, total RNA of FFPE tissues blocks was de-paraffinized, digested and extracted using RNeasy FFPE kit (Qiagen, Valentia, CA). Agarose gel electrophoresis was used to determine RNA integrity and RNA concentrations were examined by UV light Imaging System (Biorad). 200 ng of total cellular RNA were reverse-transcribed (Expand Reverse Transcriptase, Roche Diagnostics; Milan, Italy) into complementary DNA (cDNA) using random hexamer primers at 42 °C for 45 min (Random hexamers, Roche Diagnostics; Milan, Italy), according to the manufacturer's instructions. cDNA (2 μL) was amplified in a reaction mixture containing 10 mM Tris-HCl (pH 8.3), 1.5 mM MgCl₂, 50 mM KCl, 200 μM dNTPs and 2.5 U of Taq DNA polymerase (Roche Diagnostics) in a final volume of 50 μL . The reaction was carried out in a DNA thermal cycler (Applied Biosystem) [19]. The expression of the following genes were examined: ZO-1 and glyceraldehyde-3-phosphate dehydrogenase

(GAPDH) used as a housekeeping gene. The primers used for amplification were: ZO-1, 5'-caagatagttggcagcaagatg-3' and 5'-atcaggggcattcaatagcgtagc-3'; GAPDH 5'- ccacccatggcaaattccatggca-3' and 5'-tctagactggcaggcaggtcacc-3'. PCR products were analyzed by electrophoresis on 1.8% agarose gel in TBE buffer 0.5X. Densitometric analysis of agarose gel stained with ethidium bromide was carried out using Image J analysis and normalized by the housekeeping gene GAPDH. Each data point represented the mean–standard error of the mean of three biological replicates.

2.8. Barrier function analysis: TEER measurement and immunofluorescence for Claudin-1

For epithelial barrier evaluation, the I_C was withdrawn from the Mihi-oC to measure transepithelial electrical resistance (TEER) by means of Millipore-ERS (Electrical Resistance System, Millipore Corporation) as previously reported [20]. Briefly, the internal electrode was placed in the apical compartment, and the external electrode was placed in the basolateral compartment to obtain TEER value. The TEER measurements were achieved by subtracting TEER value of blank polycarbonate membranes and were presented as $\Omega \cdot \text{cm}^2$, where the surface area was calculated as the exposed apical surface of the 3D-hIs. Moreover, the quality of tight junctions was assessed by means of Claudin-1 staining. To this aim, cell samples were immune-stained for Claudin-1 and examined with Leica (Confocal Leica TCS SP5 II femtosecond laser scanning system, Leica) confocal microscope. For immunofluorescence assay of Claudin 1, the hi-oC_{LPS} and Mihi-oC_{LPS} samples were withdrawn from the Mihi-oC and fixed with 4% paraformaldehyde for 20 min and then gently rinsed with PBS. The samples were, then, incubated with a permeabilization solution (0.2% Triton X-100 + 3% BSA + PBS) for 10 min. After blocked for 1 h at RT, primary antibody (Claudin.1, 1:40, rabbit polyclonal, Abcam) was incubated for 1 h at RT. Then, secondary antibody incubation, donkey AlexaFluor 488-conjugated anti-rabbit IgG antibodies (1:250; 488 Alexa fluor), for Claudin-1 was incubated for 1 h. Cells nuclei were detected by DRAQ5 staining (5 $\mu\text{m}/\text{mL}$, Sigma Aldrich, St. Louis, MO, USA).

2.9. Stromal remodeling analyses of Mihi-oC by means of second harmonic generation imaging: collagen orientation and assembly degree analyses

All samples were collected from hi- or Mihi-oC treated or not with LPS and PBMC and investigated by confocal microscopy (TCS SP5 II Leica, Milan, Italy) combined with MPM, where the near-infrared (NIR) laser beam was derived from a tunable compact mode-locked titanium: sapphire laser (Chameleon Compact OPO-Vis, Coherent). Two-photon excited fluorescence was used to induce SHG and obtain high-resolution images of unstained collagen structures. The samples were observed in order to induce second harmonic generation (SHG) ($\lambda_{\text{ex}} = 840 \text{ nm}$, $\lambda_{\text{em}} = 420 \pm 5$) of unstained neo-synthesized collagen structures and $\lambda_{\text{ex}} = 720 \text{ nm}$. The Z-scan images were acquired with a 12 bit resolution images, 1024×1024 pixels, using a $\times 25$ water objective and were imported into Image J software to analyze the collagen degree and fibers orientation for each Z-scan. For the collagen assembly degree (CAD) examination, the intensity of the SHG signal was evaluated. The analysis was performed on all samples where the SHG signal was present. All SHG images were subjected to noise subtraction and the average intensity was evaluated as described by Eq. (5):

$$\text{CAD} \propto \bar{I} = \frac{\sum_{i=1}^{255} (I_i p_i)}{\sum_{i=1}^{255} (p_i)} \quad (5)$$

where \bar{I} is the average intensity, I_i is the intensity corresponding to the pixel p_i , while the index $i = x_i$, y_i runs in the gray value interval from 1

to 255. The intensity \bar{I} of the collagen network is known to be proportional to the degree of assembly of the newly synthesized collagen [20]. Furthermore, for collagen fibers orientation analysis, SHG images were processed by means of Image J software, using the plug-in "Orientation J" to calculate the directional coherency coefficient of the collagen fibers [21]. In details, a coherency coefficient close to 1, represented as a slender ellipse, indicates a strongly coherent orientation of the local fibers in the direction of the ellipse long axis. A coherency coefficient close to zero, represented geometrically as a circle, denotes no preferential orientation of the fibers. Representative regions of interest (ROIs) were selected from each sample, each with an area of 375 by 375 μm . Each sample was experimentally repeated three times. In each image, 5 ROI were selected for coherency analysis and the results combined. The analysis was performed in three independent experiments. Furthermore, hi-oC_{LPS} and Mihi-oC_{LPS} samples were fixed in formalin 10% and embedded in paraffin as reported above. Then, samples were cut into 5- μm -thick sections, permeabilized and unmasked with antigen retrieval. After blocked for 1 h at RT, primary antibody (Citokeratin 19, CK-19; 1:100, Abcam) was incubated for 2 h at RT. Then, secondary antibody incubation, goat AlexaFluor 488-conjugated anti-rabbit IgG antibodies, was incubated for 1 h.

2.10. Reactive oxygen species (ROS) production on Mihi-oC

All samples were collected from hi- or Mihi-oC treated or not with LPS and PBMC to assess Reactive Oxygen Species (ROS) production in the stromal compartment of 3D-hI. After the incubation, all samples were washed with PBS and incubated with 10 μM (5–6)-chloromethyl-2,7 dichlorodihydrofluoresceine diacetate (CM-DCFDA, ROS indicator, Invitrogen) at 37 °C for 60 min under dark condition. For positive control groups, the samples were incubated with H₂O₂ 400 μM for 30 min. Then, all samples were washed in PBS, returned in pre-warmed growth medium and visualized under confocal microscope (Confocal Leica TCS SP5 II femtosecond laser scanning system, Leica) using excitation appropriate source for fluorescein (FITC). For a quantitative analysis, 10 images were captured with 63 \times oil-immersion objective and ROIs with same areas were processed by using ImageJ software measuring the green fluorescence intensity. Then, the green signal (ROS indicator $\lambda_{\text{ex}} = 485 \text{ nm}$) was normalized to the surface area [22].

2.11. Cytokines profiles by ELISA assay

To analyze levels of inflammatory cytokines on 3D-hI or 3D-Mihi models after LPS treatment and flow of PBMC, 3D-hI supernatants were collected from the outlet of both upper side of the I_C and lower micro-channel and immediately frozen at -80 °C until the analysis was performed. Amounts of cytokines in each sample ($n = 3$) were analyzed using an ELISA kit pre-coated with 12 proinflammatory cytokines (Multi-Analyte ELISArray Kit for Human Inflammatory Cytokines; Qiagen, Germantown, MD) according to the manufacturer's protocol. The cytokines analyzed by this array kit include IL-1 α , IL-1 β , IL-2, IL-4, IL-6, IL-8, IL-10, IL-12, IL-17 A, IFN- γ , TNF- α , and granulocyte macrophage colony-stimulating factor (GM-CSF). Medium was collected at the Lumen and Serosal side after 6 h of LPS administration and the cytokines release profile was assayed with Elisa kit on all samples. The cytokine release profiles were normalized to cell culture respect to the control (untreated samples).

2.12. Statistical analysis

This work involved at least two replicate hi-oC or Mihi-oC per experiment. Each experiment was repeated two or three times for analyses of Live/Dead, ROS, TEER, SHG images, H&E, Alcian blue, molecular as well as inflammatory cytokine (ELISA). The results were expressed as mean ± standard deviation (s.d.) from duplicate, triplicate or more independent experiments ($n \geq 3$). In detail, for total and viable

count quantification analyses, turbidimetric measurement or viable counts of bacterial suspensions was performed in triplicate and repeated at least three times for each time point. For Live/Dead quantitative analysis, 5 digital images were divided in at least 5 regions of interests (ROIs) with comparable areas and analyzed with Image J software. For section staining (histological, SHG) three samples were used for each experimental phase and 10 sections, were used per sample, then about five ROIs were examined for each section and processed with Image J software. In detail, for mucus deposition analysis, 10 sections were used and at least five different fields were randomly examined in each section by using color deconvolution plugin of Image J software, reporting the mean percentage of blue stained region. For the villi thickness, 10 H&E-stained sections were selected and analyzed with Image J software. For TEER measurements, the analysis was performed in triplicate on hI-oC and MihI-oC treated or not with LPS and PBMC and repeated at least three times. For coherency coefficient measurements, SHG images were collected and about 5 ROIs were examined for each section with Image J software. For CAD and ROS measurements hI-oC and MihI-oC treated or not with LPS and PBMC were processed with Image J software by measuring gray signal in representative ROIs selected from each sample or green fluorescence intensity of 10 images for each sample, respectively. For molecular analyses the quantification was expressed as total rDNA amount expressed as ng/mL or normalized to 100% (for bacteria) or as a fold-change relative to gene expression of the control groups (for epithelial cells) and quantified with Image J software. Three independent experiments in triplicate were performed. The cytokine release profiles was quantified on 3D-hI or 3D-MihI models after LPS treatment and flow of PBMC with OriginPro software and normalized to cell culture. All results were then statistically analyzed by the Student's t-test. The differences between two or more groups were evaluated by using one-way analysis of variance (ANOVA) followed by the Tukey's post-test by using OriginPRO software. Statistical significance was set at a value of $p < 0.05$. The values were outlined in the figure legends.

3. Results and discussion

In recent years, microfluidic intestine on chips were established considering multiple system parameters such as oxygen concentration and fluid flow including also more comprehensive functionality, such as villi-like structures, intestinal peristalsis, oxygen gradients, and even immune systems. Recent gut-on-chip models also investigated the role of microbiota in maintaining intestinal health and immune regulation emulating *in vitro* the physiology of the human gastrointestinal tract [23, 24]. Here, we reproduced the mucosal-associated microbiota-cell interactions into the complex microenvironment of an immune-responsive Microbiota-human Intestine axis on-chip in which microaerophilic and obligate anaerobic microbiota species are vertically stratified within the mucus overlying the epithelium of the 3D-hI. In contrast to the intestinal epithelium model grown on the exogenous membrane, here, the 3D-hI presents an instructive and histologically competent ECM and a well-differentiated epithelium with mucus-covered microvilli. This physiological context allows to investigate the impact of microbiota on the 3D-hImorphology and functional performance in terms of barrier protein and mucus production as well as the microbiota-epithelial/stromal-immune system cross-talk. The complex ECM featuring the intestinal lamina propria has a fundamental role in dictating the epithelium morphogenesis as well as the microbiota adhesion and stratification. Moreover, we replicated the microenvironmental anaerobic condition of the human intestinal lumen by providing the MihI-oC with a custom-made M_C that allow to establish the physiological hypoxic environment in the small intestine. In this condition we were able to replicate, for the first time, the physiological oxygen dissipation along the thickness of the 3D-hI from the serosal side of the lamina propria to the luminal side where microbiota was grown. Furthermore, we improved the complexity of the intestinal extracellular microenvironment by integrating cell populations that are directly

involved in the inflammatory response (two species of the intestinal commensal microbiota on the lumen side and PBMCs on the serosal side). We evaluated the geographical change as well as the protective role, immunomodulation, and immune-tolerance maintenance of the microbiota in LPS-induced barrier impairment and the indirect role of the microbiota on stromal reshaping in response to the inflammatory stimulus. Finally, we evidenced the synergistic contribution of different cell populations such as epithelial, stromal, blood, and microbial species on the release of the key immune mediators (pro- and anti-inflammatory cytokines, ROS).

3.1. Establishing hypoxic environment in microbiota chamber (M_C) of MihI-oC

Healthy intestinal mucosa is able to sustain physiological oxygen concentrations much lower than atmospheric conditions causing a horizontal steep oxygen gradient along the length of the intestine and a vertical gradient from the severely oxygen deficient lumen to the highly vascularized and oxygenated serosa [25,26]. Commensal facultative anaerobic and microaerophilic bacteria inhabiting the lumen and epithelial mucosa are strictly involved in the establishment of the luminal physiological hypoxia condition called "physioxia" [27]. On the other hand, obligate anaerobic bacteria colonize the near anoxic microenvironment at the midpoint of the lumen establishing a stratification of the bacterial communities along the radial axis of the small intestine [28]. Therefore, any attempts to recapitulate *in vitro* the gut-microbiota axis have to mimic the anoxic-oxic interface of the intestinal lumen that is a key element of the gut microenvironment for the survival of the commensal microbiota as well as for the formation of a functional epithelial barrier. Here, we replicated the microenvironmental anaerobic condition of human intestinal lumen by fabricating a custom-made M_C allowing us to establish on the apical side of the 3D-hI, the physiological near-anoxia microenvironment (<0.0013% O₂) existing at the midpoint of the intestinal lumen that is the mandatory condition for the colonization of the obligate anaerobic bacteria [28]. Comsol Multiphysics was used to simulate the oxygen concentration, in a given point of the M_C , by changing the flow rates at which N₂ was flushed inside the M_C (Fig. 1a and b), to determine the amount of time necessary to eject free oxygen outside the M_C to produce a near-anoxia environment. Real-time and non-invasive measurements of the oxygen concentration were carried out by setting up the MihI-oC in the configuration reported in the Fig. 1c, by using an oxygen optical detector [9]. During the measurement, the culture medium flow rate was set at 30 μ L/min at the S_C and the N₂ flow rate at 200 μ L/min, the result is reported in the Fig. 1a, (purple empty circles in the graph) and confirmed the Comsol simulation at the same N₂ flow rate (purple continuous line). In addition, the results of the simulations displayed that the highest tested N₂ flow rate (400 μ L/min) generated a near-anoxia environment inside the chamber within just 5 min. However, this flow rate created turbulent flow with visible formation of surface waves, which invalidated the bacterial viability. Conversely, lowering N₂ flow rate at 200 μ L/min, the turbulent flow was prevented and the near-anoxia environment, as calculated by Comsol simulation, was reached in 15 min (Fig. 1d-f; Time 0 (d), Time 7 min (e), Time 15 min (f)).

Remarkably, this value is still a lower time as compared to other intestinal on-chip models in which the time to reach the opportune near-anoxia environment is almost doubled [9]. According to Einstein-Smoluchowski equation for diffusion of gases in solution ($t = 0.5 \cdot r^2 \cdot D^{-1}$), where r equals the height of 200 μ L of microbiota side into the device (5 mm) and D is the diffusion coefficient of O₂ ($2.46 \cdot 10^{-9} \text{ m}^2 \text{s}^{-1}$), the expected time required for oxygen to diffuse across microbiota was calculated as ~ 85 min. So, to prevent the re-oxygenation of the M_C , instead of completely stopping N₂ flow after reaching near-anoxia microenvironment, N₂ was kept flushing at very low flow

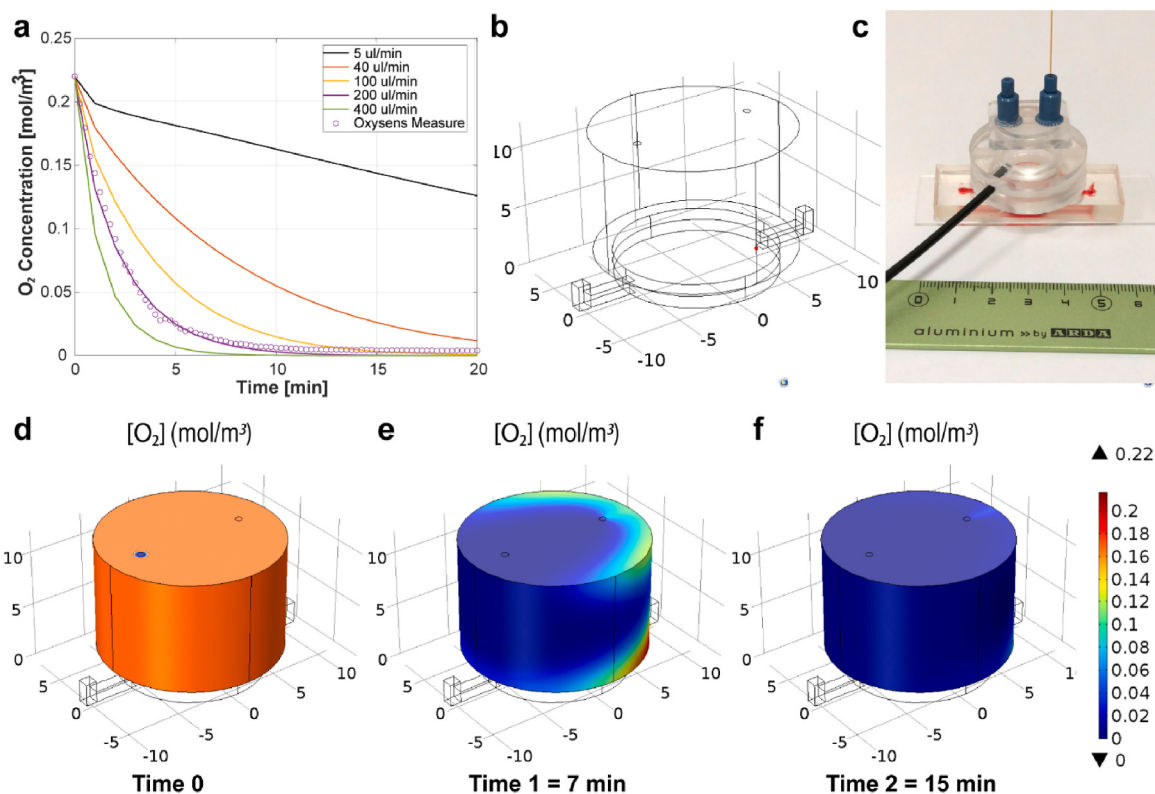


Fig. 1. Design and optimization of flow rate of M_C . Continuous lines indicate oxygen concentration at various N_2 flow rates calculated by Comsol simulation, purple empty circles indicate the values of the real-time measurements obtained by using an oxygen optical detector (a); schematic representation of M_C , the red mark indicates the point at which the oxygen concentration was measured by Comsol simulation (b); experimental setup of on-line measurement shows a support for optical fiber accommodation (c); Comsol simulation indicates the reduction of the oxygen concentration in the whole volume of the M_C at a flow rate of $200 \mu\text{L}/\text{min}$ at different time points: Time 0 (d), Time 7 min (e), Time 15 min (f). (For interpretation of the references to color in this figure legend, the reader is referred to the Web version of this article.)

rate such as $5 \mu\text{L}/\text{min}$ for the entire duration of the experimental phase (Supplementary Figure. S6). Even if N_2 comes in the M_C at 24°C , the time required from the system to reach the optimal temperature of 37°C is in order of few minutes (8 min) as measured by a hand-made Arduino set-up (Supplementary Figure. S5). Therefore, any issues for the bacterial viability and growth occurred. Then, a flow of oxygenated medium was streamed at $30 \mu\text{l}/\text{min}$ into the serosal channel (S_C) of the Mihi-oC to provide the stromal side of the 3D-hI with the necessary nutrient and oxygen (see Table 1).

3.2. Microbiota chamber (M_C) promotes microbial strains growth and oxygen gradient across the Mihi-oC lumen

Of note, the microbiota is biogeographically stratified within the gastrointestinal tract on different spatial scales and axes and its viability is strictly dependent on the luminal-serosal oxygen gradient. To fully understand the functionality of the intestinal microbiota, great attention must be paid to the microhabitats within the intestinal ecosystem and the spatial relationships among microorganisms and between microorganisms and the host [4]. In particular, vertical stratification of the microbiota was revealed along the crypt-villus axis changing from the surface of the macrovilli and crypts colonized by adherent species and the epithelium colonized by obligate anaerobic bacteria completely embedded within the mucus [4,5]. This bacterial stratification is strictly related to the intraluminal oxygen gradient that influences the spatially heterogeneous growth of the microorganisms as well as the intestinal tissue functionality. Studies reported the optimal O_2 profile at various locations along the radial axis of the intestinal lumen ranging from the normoxic submucosa ($0.15 \text{ mol}/\text{m}^3$), to the low oxygen environment along the crypt villous axis ($0.07\text{--}0.03 \text{ mol}/\text{m}^3$) with a hypoxic

environment at the tip of the villi ($0.03 \text{ mol}/\text{m}^3$) to the near anoxia at the distant lumen as reported in Table 2 [28]. In this perspective, to assess the capability of M_C to guarantee microbiota viability and growth as well as to reproduce its correct topographical vertical distribution on the intestinal lumen (Fig. 2a), anaerobic (*B. longum*) or microaerophilic (*L. rhamnosus*) strains were cultured on the luminal side of the 3D-hI, housed in the I_C of the Mihi-oC (Fig. 2b and c). While continuous N_2 flow assures the anaerobic condition into M_C , the oxygenated

Table 1
Mathematical modeling parameters.

Variable	Description	Value	Source
μ^f	Dynamic viscosity of the fluid (culture media) (Pa s)	0.001	[15]
μ^t	Effective viscosity of the fluid in the tissue domain (Pa s)	0.0016	[15]
ϵ	Porosity of the tissue	0.7	[15]
κ^t	Effective hydraulic conductivity (m^2)	10^{-11}	[15]
D^f	Oxygen diffusivity in the culture media (m^2s^{-1})	10^{-9}	[15]
D^t	Oxygen diffusivity in the tissue (m^2s^{-1})	10^{-10}	[15]
C_0	Equilibrium oxygen concentration in the culture media (μM)	0.22	[15]
ρ	Cell per μTPs (cell m^{-3})	$0.2\text{--}10^{14}$	[16]
V_{max}	Maximum rate of oxygen consumption ($\text{mol cell}^{-1}\text{s}^{-1}$)	10^{18}	[16]
K_m	Oxygen concentration at 0.5 (V_{max}) (μM)	10^3	[16]
K_{dv}	Dynamic permeability (m^2)	0	[16]
R	Oxygen consumption rate ($\mu\text{M s}^{-1}$)	$\frac{V_{max}C}{K_m + C}$	[16]
D^a	Oxygen diffusivity in the PMMA (cm^2s^{-1})	10^{-8}	[17]
C_{0-a}	Equilibrium oxygen concentration in the anaerobic chamber (μM)	0.01	[18]

Table 2

Definition of relevant oxygen environments at 37 °C into Mihi-oC.

Localization	O ₂ [mol/m ³]	pO ₂ [kPa]
Serosal side	0.21	19.9
3D-IS	0.15	7
3D-hI (Crypt-villus)	0.03–0.07	3–0
Lumen side	0.001	0.13–0.013

antibiotic-free medium was flowed into the S_C of the Mihi-oC to provide the adequate oxygen supply to allow human intestinal cells viability. In this way, an oxygen gradient across the Mihi-oC was established, so providing a physiological microenvironment with a functional host-microbiota interface and vertical bacteria stratification. CFD fluidodynamic simulation was performed and reported in [Supplementary Figure. S3-S4](#), in order to identify the optimal medium flow rate to ensure the correct oxygen supply to the cells reproducing the physiological oxygen level of the small intestinal wall, which is ~0.22 mol/m³ [28]. CFD simulation revealed that, when culture medium was flushed at 30 µL/min, a right compromise between oxygen amount in the 3D-hI hosted in the Mihi-oC (0.22 mol/m³ at the bottom) and shear stress (0.0267 dyne/cm²) was obtained ([Figure. S3b and e, S4b](#)). Moreover, CFD of the full-assembled Mihi-oC was performed to simulate fluid dynamic condition and oxygen provision inside the whole system when oxygenated culture medium was flushed at 30 µL/min in the bottom part of Mihi-oC (serosal microchannel) and N₂ was injected at 5 µL/min in

the M_C (after the initial emptying of the M_C at µL/min) ([Fig. 2d-f](#)). In [Fig. 2d](#), it is showed the oxygen gradient extending from the 3D-hI throughout the mucosal interface into the lumen, whereby microorganisms adjacent to the epithelium of 3D-hI consume most of the available oxygen, keeping the bulk of the lumen deeply hypoxic. We replicated, for the first time, *in vitro*, the physiological oxygen dissipation occurring along the thickness of human small intestine from the serosal side of the lamina propria to the luminal side where microbiota was grown. These conditions provide an environment in which the endogenous ECM produced in our 3D-hI is able to guarantee the regulatory function of the native lamina propria providing the instructive conditions that *in vivo* maintain the microbiota adhesion and stratification. [Fig. 2e](#) showed the oxygen gradient from the serosal side to the villi tips of the Mihi-oC with a hypoxic lumen that host microaerophilic bacteria and the near-anoxic apical side of the M_C in which the obligate anaerobes grow embedded into an endogenously produced mucus layer, reproducing the correct extracellular microhabitat of the small intestine. Furthermore, [Fig. 2f](#), showed that a fully developed Poiseuille velocity profile was established in the S_C and a uniform N₂ velocity (0.0001 m/s) was established in the M_C. These conditions were safe for cell and bacteria viability. In order to demonstrate the M_C functionality in comparison to the conventional culture methods in bacterial glove box, the growth curve of the microaerophilic (*L. rhamnosus*) or anaerobic (*B. longum*) strains cultured in three different conditions for 36 h were estimated: 1) micro-AW, 2) ana-AW, 3) hypoxic environment in the Mihi-oC. Differences between total and viable bacteria were reported

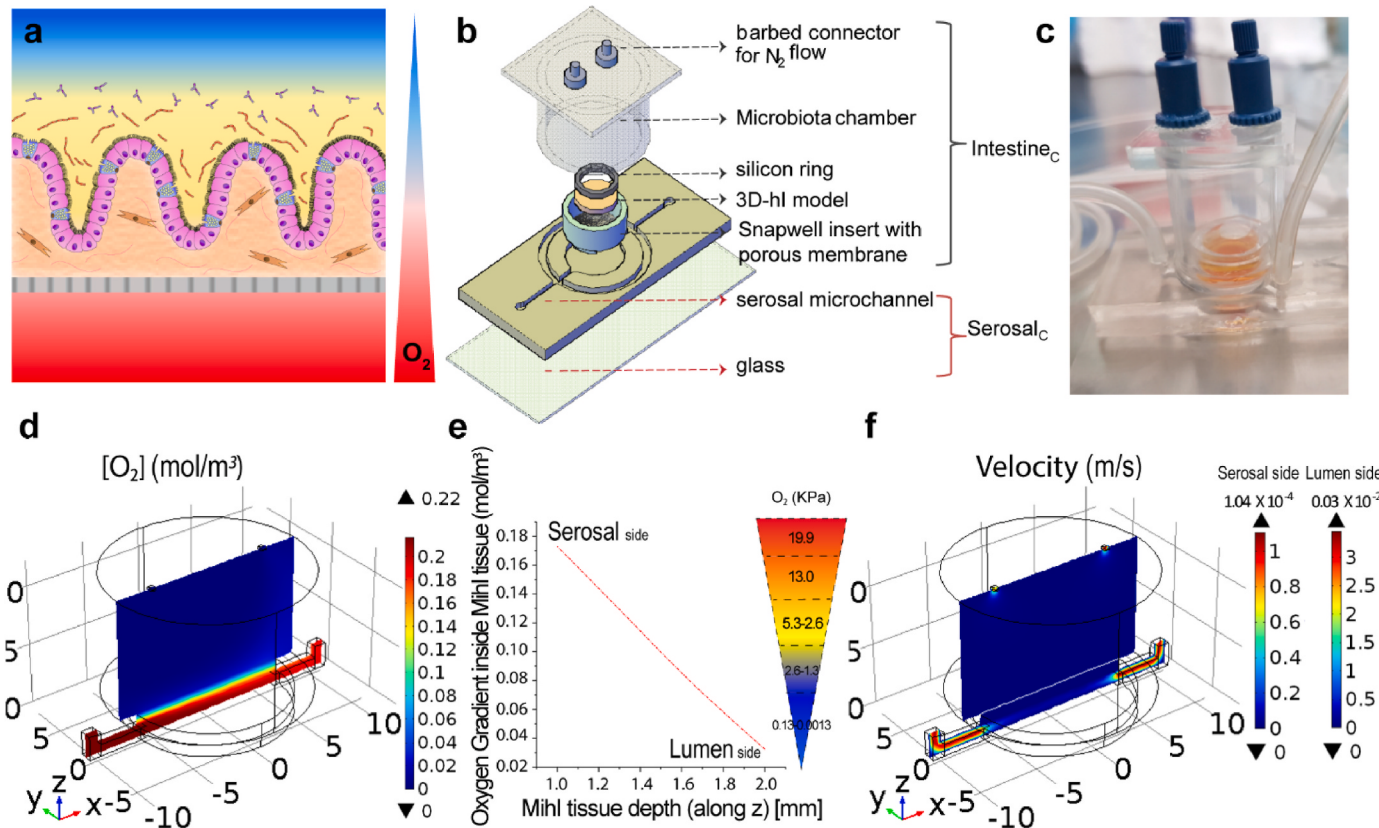


Fig. 2. Mihi-oC establishes the physiological oxygen gradient across the Mihi tissue. Schematic representation of the transversal section of Mihi-oC with fibroblasts embedded into the auto-produced ECM overlaid by a polarized and differentiated epithelium and the vertically distributed microbial strains into the luminal side; a triangular color map indicates the oxygen gradient from the Serosal side to the Lumen side (a); rendering of the Mihi-oC highlights the I_C and S_C separated by a porous membrane (b); experimental setup of Mihi-oC highlights the M_C that seals the I_C in which was accommodated the 3D-hI (c); Comsol simulation indicates the oxygen concentration field in the Mihi-oC by using medium flow rate at 30 µL/min into the S_C and N₂ flow rate at 5 µL/min at the inlet of M_C (d); the graph reports the oxygen dissipation along the thickness of Mihi-oC from the S_C of the lamina propria to the Luminal side where microbiota grows; the colour map shows the oxygen tension (ranging from 19.9 KPa at Serosal side to 0.13–0.0013 KPa at Lumen side) into Mihi tissue depth along the z axis (e); Comsol simulation shows the velocity profile into the entire setup of Mihi-oC (f), the color maps indicated the Serosal and the Lumen side, respectively.. (For interpretation of the references to color in this figure legend, the reader is referred to the Web version of this article.)

compared to the standard curve generated under conventional growth conditions, which are micro-AW for *L. rhamnosus* and ana-AW for *B. longum*, respectively. As pointed out in the inset of Fig. 3a, differences in the lag phases between the growth condition in micro-AW and the Mihi-oC were displayed, due to the *L. rhamnosus* growth adaptation into the M_C, in which an oxygen gradient from the basal to the apical side, with a progressive reduction of oxygen going upwards, was found. In fact, the bacteria prolonged the lag phase, but subsequently they self-adapted to the oxygen gradient condition in the M_C. Further, once adapted to the growth condition into the M_C, the exponential growth phase was completely superimposed on that of the micro-AW. Additionally, the stationary phase lasts longer in the Mihi-oC before reaching the death phase. *L. rhamnosus* grown under ana-AW showed a growth curve having the same trend but with lower values at each time points (Fig. 3a). For *B. longum* cultured in ana-AW, the curve of total bacteria is completely superimposable to that in Mihi-oC with slightly higher values of the viable bacteria in the device probably due to the CO₂ concentration coming from the basal side or from the exchange of CO₂ in the incubator. It is already known, indeed, that CO₂ although in small percentage can positively influence the growth of the *B. longum* [29,30]. A strong reduction of total bacteria concentration was reported in micro-AW condition due to the O₂ exchange during the culture time. In ana-AW, the lag phase overlapped with slight differences in the enrichment of the plateau (log phase). Slight increase of the live bacteria in the Mihi-oC compared to ana-AW was shown, due to the optimal microenvironment provided into the M_C of the Mihi-oC as showed in the Fig. 3b. All data were compared with viable count of each strain at different times of culture (Supplementary S7a and b). In aerobic

conditions, a significant reduction of *L. rhamnosus* and no colony growth for *B. longum* was found (data not shown). Finally, the bacterial samples were collected from Mihi-oC during the log phase and histological as well as ultrastructural characterization was performed (Supplementary Figure. S7c and d, and insets). The bacteria viability under different culture conditions was also confirmed by on-line measurements of Live/dead staining during log phase of culture (Supplementary Figure. S8). Representative Live/Dead images of single strain grown (*L. rhamnosus* and *B. longum*) in Mihi-oC under optimal growth conditions indicated the bacterial growth >90% for both strains (Fig. 3c and d, respectively) preserving the bacterial morphology as highlighted by high magnification images (Fig. 3c and d, insets). Quantitative analysis of Live/Dead staining did not show significant differences when the single bacterial strain in the log phase were grown in the Mihi-oC compared to their optimal growth conditions in AW (90 ± 2.2% and 89 ± 2.7 respectively for *L. rhamnosus*; 87 ± 1.5% and 91 ± 2.4% respectively for *B. longum*). A strong significant reduction in cell viability was evidenced for *B. longum* in micro-AW confirming the viable count data (Fig. 3e, S8).

3.3. Establishing physiological vertical localization of microbiota in Mihi-oC

Once established the Mihi-oC micro-milieu, the in-depth histotypical, molecular and ultra-structural analyses were carried out to deeply investigate the co-culture of 3D-hI with the bacterial strains. Differently from the gut-microbiota on chip models previously proposed [7–9,31], here the 3D-hI is a complex tissue model (Fig. 4a) composed

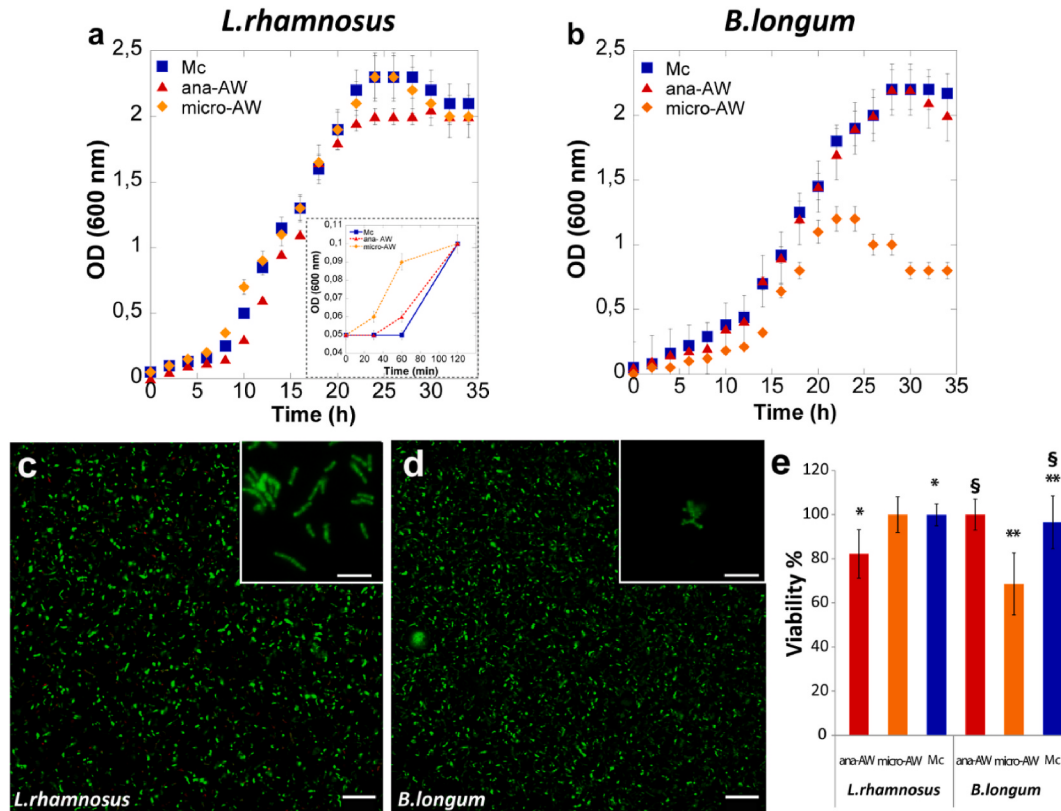


Fig. 3. Microbiota Chamber (M_C) sustains the microbial strains viability and growth in the Mihi-oC lumen. Quantification of total viable bacterial growth - *L. rhamnosus* (a) and *B. longum* (b) - on different oxygen microenvironments: microaerophilic conditions in the AW (micro-AW), anaerobic conditions in the AW (ana-AW), hypoxic environment in the M_C of the Mihi-oC (M_C); the inset indicates the Lag phases difference between *L. rhamnosus* growth in micro-AW, M_C and ana-AW (a, inset). Micrographs of the on-line monitoring of viable bacteria (Live/Dead staining) shows the optimal culture conditions for each bacterial species - *L. rhamnosus* (c) and *B. longum* (d) with high magnification insets that depict the microbial morphology; scale bar 75 µm for c and d, scale bar 20 µm for insets; the graph reports the quantitative analysis of live bacteria on different oxygen microenvironments. Data are presented as mean ± SEM of three separate experiments, each one performed in triplicate (n = 9), *p < 0.001, **p < 0.01, §p < 0.05 (e).

by an endogenously cell-produced ECM on which intestinal villi-like protrusion covered by a well-polarized epithelium is strictly adhered (Fig. 4b, *). Recent evidences demonstrated a key role of intestinal lamina propria, not only on the epithelium morphogenesis [11,12,14, 20] but also on microbiota adhesion, distribution and growth [32]. Here, as first step toward the reproduction of intestine-microbiota axis, single bacterial strain was co-cultured on 3D-hI in Mihi-oC, and histological characterization (H&E and alcian blue staining) confirmed the correct localization of each strain. We found the microaerophilic *L. rhamnosus* adhered on the polarized microvilli (Fig. 4b black arrowhead) and the anaerobic *B. longum* vertically distributed far from the epithelium (Fig. 4c black arrowheads). Moreover, abundant mucus overlying the intestinal epithelium was detected (Fig. 4d and e, * inset, Supplementary Figure. S9 and S10). Emerging evidences reported the intestinal mucus layer as the first line of defense against the bacterial infiltration and the physical barrier to antigenic substances, digested food particles, enzymes and acids into the lumen [33]. Moreover, the bacterial adhesion to intestinal mucus and epithelia seems to be important for individual stability of the microbial flora [5]. In fact,

intestinal bacteria have adapted to colonize the mucus layer by adhering to intestinal mucus components, using mucus-derived nutrients, and sensing chemical cues for adaptation. We have previously demonstrated the relevance of the stromal signals in driving the Caco-2 cells to differentiate in mucus-producing cell phenotype without any exogenous stimulus and the failure of the mucus production in 2D transwell culture [14]. Here, we demonstrated that in our Mihi-oC a complex environment was reproduced comprising the mucus layer with embedded bacteria. Transversal section of alcian blue-stained samples confirmed the presence of adherent *L. rhamnosus* on the apical surface of the polarized epithelium as well as in the neo-produced mucus blanket by goblet-like cells as highlighted by the high magnification image (Fig. 4d marked with *). In addition, *B. longum* strain resulted completely embedded into the mucus layer detached from the epithelium stained in blue (Fig. 4e). In order to prove the topographical distribution of the bacterial strains cultured on the luminal side of the Mihi-oC, quantitative analysis of 16 S ribosomal DNA (rDNA) from tissue supernatant (reported as no adherent) or scratched from the apical surface of the epithelial cells (reported as adherent) was assessed. As described in Fig. 4f, a high

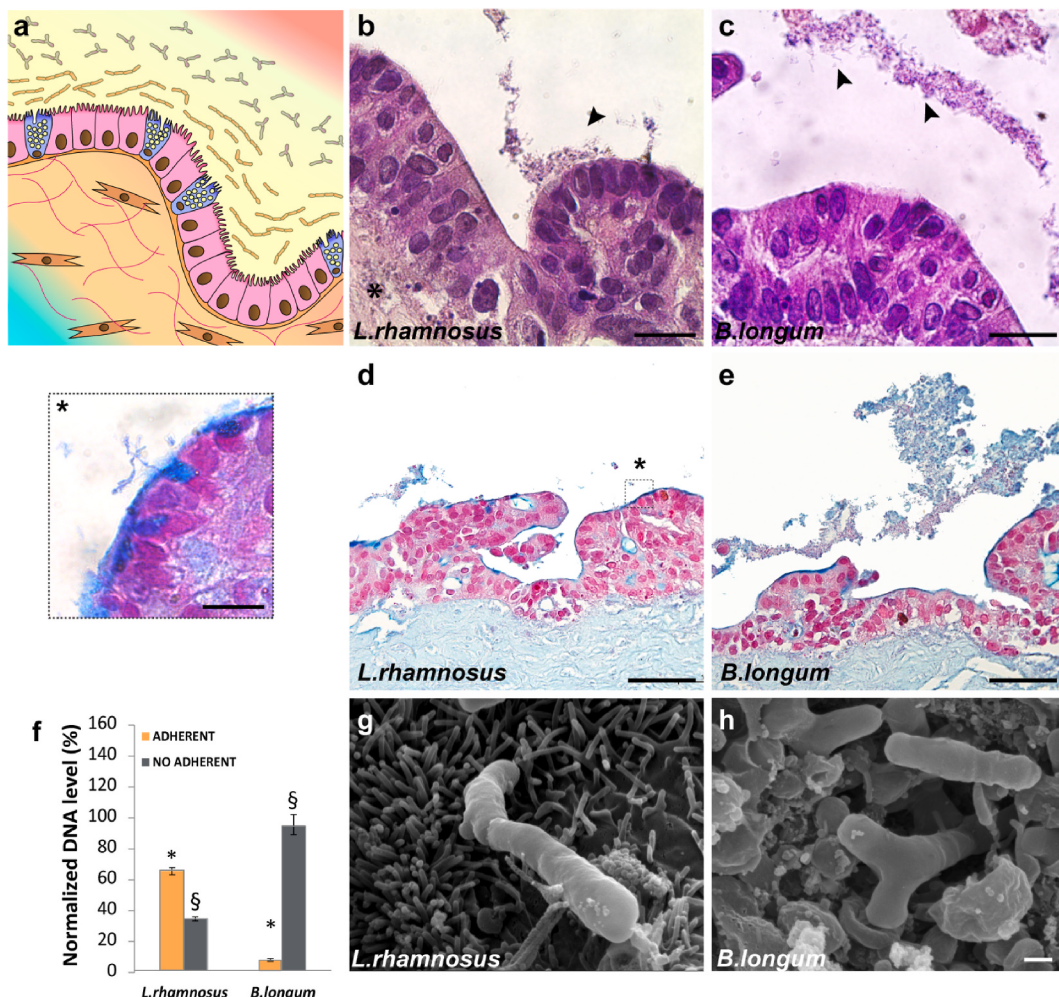


Fig. 4. Physiologic condition in the lumen of Mihi-oC determines the physiological vertical stratification of the microbiota. Schematic representation of villous tip indicates the geographical distribution of the microbial species into the Lumen side of the small intestine (a); representative high magnification H&E images of 3D-hI shows the *L. rhamnosus* adhesion on the apical side of the epithelial cells (b) and *B. longum* away from the epithelium (c), scale bar 20 μ m; alcian blue stained section of 3D-hI depicts the mucus producing cells and the *L. rhamnosus* adhesion on mucus that cover the microvilli (d and inset *; scale bar 200 μ m and 20 μ m, respectively) and *B. longum* completely embedded into the mucus far from the epithelium (e, scale bar 200 μ m); bars diagram indicates the DNA level of two bacterial strains reported as adherent and non-adherent; samples groups were compared: adherent vs non-adherent, *L. rhamnosus* vs *B. longum* with * $p < 0.001$, § $p < 0.05$ (f); high magnification SEM micrograph evidences the *L. rhamnosus* adhesion on microvilli structures (g) and *B. longum* immersed into the mucus (h), scale bar is 200 nm. Data are presented as mean \pm SEM of three separate experiments, each one performed in triplicate ($n = 9$). (For interpretation of the references to color in this figure legend, the reader is referred to the Web version of this article.)

amount of the 16 S rDNA sequences of *B. longum* was detected into the supernatants that contains unbounded bacteria immersed into the mucus layer. Conversely, a low amount of rDNA of *B. longum* was revealed on scratched supernatants confirming the correct topographical location of this strain, that due to its anaerobic nature is physiologically found far from the oxygen enriched-epithelial cells. In contrast, a small amount ($25-35 \pm 3.5\%$) of rDNA of *L. rhamnosus* was found in the supernatant collected in the lumen of the 3D-hI (no-adherent). In agreement with literature [34], high amount of rDNA sequences of *L. rhamnosus* were found in the scratched supernatants indicating that the *L. rhamnosus* is preferentially localized on the surface of the microvilli of the epithelial cells. In addition, the ultra-structural images showed that the *Lactobacilli* preserved their morphology and colonized the hI-oC along the Crypt-villous axis. SEM micrograph reported that most microaerophilic bacteria (*L. rhamnosus*) adhered directly on the apical surface of the epithelial cells and are lodged on the brush border structures as showed in Fig. 4g and Supplementary Figure S10a. Conversely, representative SEM image of *B. longum* demonstrated that the bacteria were completely immersed into the mucus layer produced by the Goblet-like cells of the hI-oC (Fig. 4h and Supplementary Figure S10b).

3.4. Induced-intestinal barrier dysfunction on immune-responsive MihI-oC

As recognized, the mucosal immune system establishes a physical as well as dynamic barrier against external mediators including antigens and pathogens exerting control mechanisms to maintain intestinal homeostasis [35]. An alteration of this equilibrium predisposes to inflammatory diseases of the gastrointestinal tract, such as Inflammatory Bowel Diseases (IBD). We previously demonstrated the contribution of the stromal microenvironment (myofibroblasts and ECM proteins) in innate immune response under inflammatory stimulus [12]. Here, we analyzed the response to inflammatory stimulus in a more complex luminal/serosal extracellular microenvironment in order to elucidate the contribution of multicellular components on the onset of inflammation. To recreate the inflamed-MihI-oC (MihI-oC_{LPS}) system (Fig. 5a), we introduced high dose of LPS from *E. coli* (15 $\mu\text{g}/\text{mL}$) - known to produce adverse effects on the intestinal barrier integrity [36] - to the luminal compartment of the MihI-oC enriched with both microbiota species (*L. rhamnosus* and *B. longum*). Meanwhile freshly isolated PBMC were introduced in the S_C to provide the system with the immune-responsive cells. Some previous works reported that the intestinal inflammatory diseases determine the destruction of intestinal villi and as consequence compromises the intestinal permeability barrier, which is believed to result from the complex pathological interplay between the intestinal epithelium, gut microbes, and immune cells [37]. Here, the microbiota/3D-hI morphology and functional performance as well as the microbiota-epithelial/stromal-immune system cross-talk were evaluated by means of immune-hystotypical, TEER and molecular analyses. Histological characterization of the un-inflamed tissue samples with or without microbiota (respectively MihI-oC and hI-oC) collected from the chip showed a polarized epithelium with epithelial cells firmly connected to neighboring ones in both Fig. 5b and c. The latter shows the microbiota colonization on the luminal side of the polarized epithelium indicated by black arrows. In contrast, when inflammation was induced by LPS, in absence of microbial colonization (hI-oC_{LPS}) a substantial damage of the barrier integrity and loss of the brush border occurred as evidence by histological images, in which the detachment of the epithelial cells that assumed a spherical shape, is indicated by black arrowheads (Fig. 5e). This impaired condition is partly stemmed when microbiota is present, as highlighted by the comparison between hI-oC_{LPS} and MihI-oC_{LPS} (Fig. 5e and f, respectively). Moreover, the protective role of the microbial species in preserving the villi-like structure is evidenced by the quantitative measurement of the height of the macrovilli-like structures (Fig. 5d) and by the tightness of the epithelium. However, very small areas showed

the bacterial translocation into the injured regions (Fig. 5f, black arrow and Fig. 5g, high magnification image, Supplementary Figure S11) suggesting that the inflammatory stimulus partially compromises the epithelial barrier in the MihI-oC_{LPS} + PBMC inducing the tight junction-opening mimicking a pathogenic infection of Gram-negative bacteria only in a restricted area. Interestingly, the presence of some immune cells (with an average size between 6 and 8 μm) on the stromal side of the MihI-oC_{LPS} suggesting that LPS stimulation elicited the immune cell recruitment, probably mediated by microbial, epithelial and stromal inflammatory cytokines release [38] (Fig. 5h, Supplementary Figure S12a and b). This is in agreement with some studies investigating the impact of the microbiome of the gastrointestinal tract on the immune response [39]. In addition, an evident immunofluorescent positive signal for the tight junction protein Claudin-1 was reported in MihI-oC_{LPS} compared to the pixelated signal in hI-oC_{LPS} (Fig. 5i and j, respectively), further confirming a role of microbiota in reducing dysfunction of the epithelial barrier in MihI-oC_{LPS}, although quantitative analysis was not operable due to the bacterial fluorescence interference. In this perspective, to quantitatively estimate the barrier integrity in terms of the intestinal tight junctions opening, TEER measurement were also performed. As expected, the un-inflamed 3D-hI expressed higher TEER values ($318 \pm 3.6 \Omega^*\text{cm}^2$) compared to hI-oC_{LPS} ($210 \pm 12 \Omega^*\text{cm}^2$) (Fig. 5k), indicating a TEER reduction of about 66% caused by pathogenic stimulus. The presence of microbiota (MihI-oC), *per se*, significantly increases the TEER value ($710 \pm 12 \Omega^*\text{cm}^2$) regardless the microbiota was composed by single strain or both (*L. rhamnosus* and *B. longum*) (Supplementary Figure S13). When LPS was added on MihI-oC, a mild decrease (14%) of TEER values was found ($613 \pm 10 \Omega^*\text{cm}^2$). The little fall of the TEER value between MihI-oC_{LPS} and MihI-oC, further confirm the protective role of the microbiota on the intestinal barrier function. Molecular quantification of ZO-1 mRNA level was also performed indicating that the LPS treatment led to a decrease of ZO-1 gene expression on hI-oC_{LPS}, whereas the presence of microbiota - that *per se* increases the tight-junction gene expression and the TEER value as well - allowed high level of junctional gene expression (Figure. 5l). It is noteworthy that non-mucin-degrading *B. longum* improves mucosal health and barrier due to its ability to promote the proliferation of goblet cells as well as to stimulate the mucus production, glycosylation and expulsion [40]. Accordingly, we showed an over-production of the intestinal mucus quantified by alcian blue staining on MihI-oC_{LPS} samples compared to microbial-free samples (hI-oC_{LPS}) (Figure 5m). It is noted that the microbiota vertical stratification was compromised in inflamed gut [4]. We argue that high amount of LPS compromises the microbial diversity in terms of vertical stratification (Fig. 6a) as well as total bacterial amount in MihI-oC_{LPS} compared to un-inflamed one (Fig. 6b). In details, molecular analysis revealed a significantly compromised vertical bacteria distribution after LPS treatment. Indeed, compared to the un-inflamed condition, in the MihI-oC_{LPS} we found a turned localization of *L. rhamnosus* with a great rDNA amount of the no-adherent bacteria, therefore immersed into the mucus, and a low rDNA amount adherent on the epithelium. An overgrowth of the *B. longum* species was also highlighted by an increase of rDNA level in both mucus-embedded bacteria and epithelial-deposited bacteria in MihI-oC_{LPS}. At last, a reduction in total microbiota amount was registered for un-inflamed MihI-oC compared to MihI-oC_{LPS} mainly due to the overgrown of *B. longum*.

3.5. Stromal reshaping in immune-responsive MihI-oC

In order to demonstrate the contribution of the multicellular population on the onset of inflammation, analyses of the stromal compartment in terms of collagen fibers orientation, ECM remodeling and ROS production under physio- or pathological stimulus were performed with or without microbiota colonization and with or without PBMC flow in hI-oC_{LPS} or MihI-oC_{LPS}. In general, the gut models proposed in literature lack the stromal compartment at all, or it is represented by an exogenous

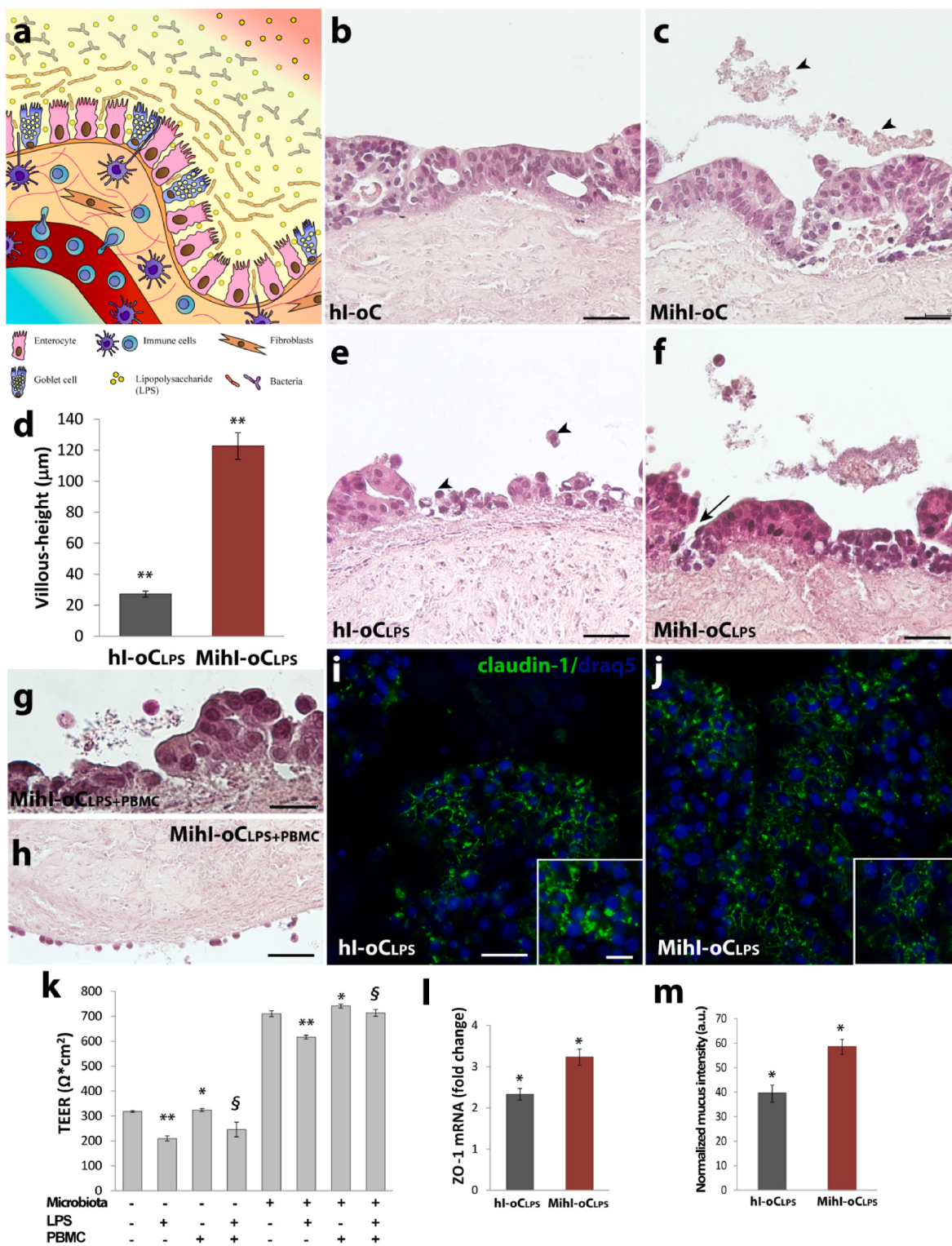
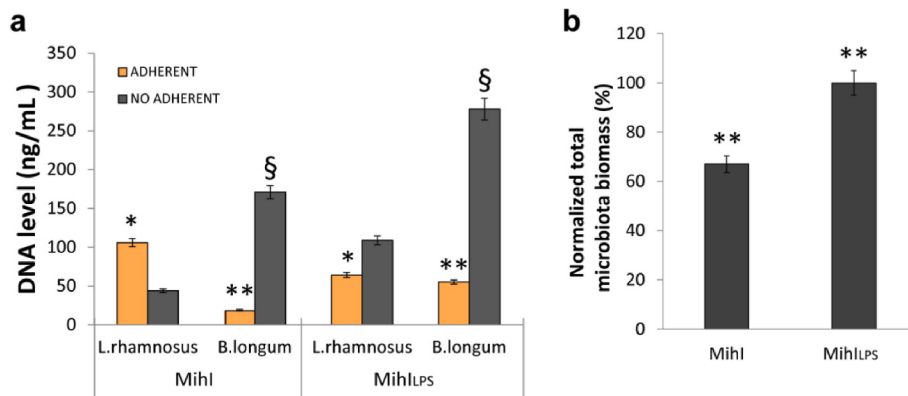
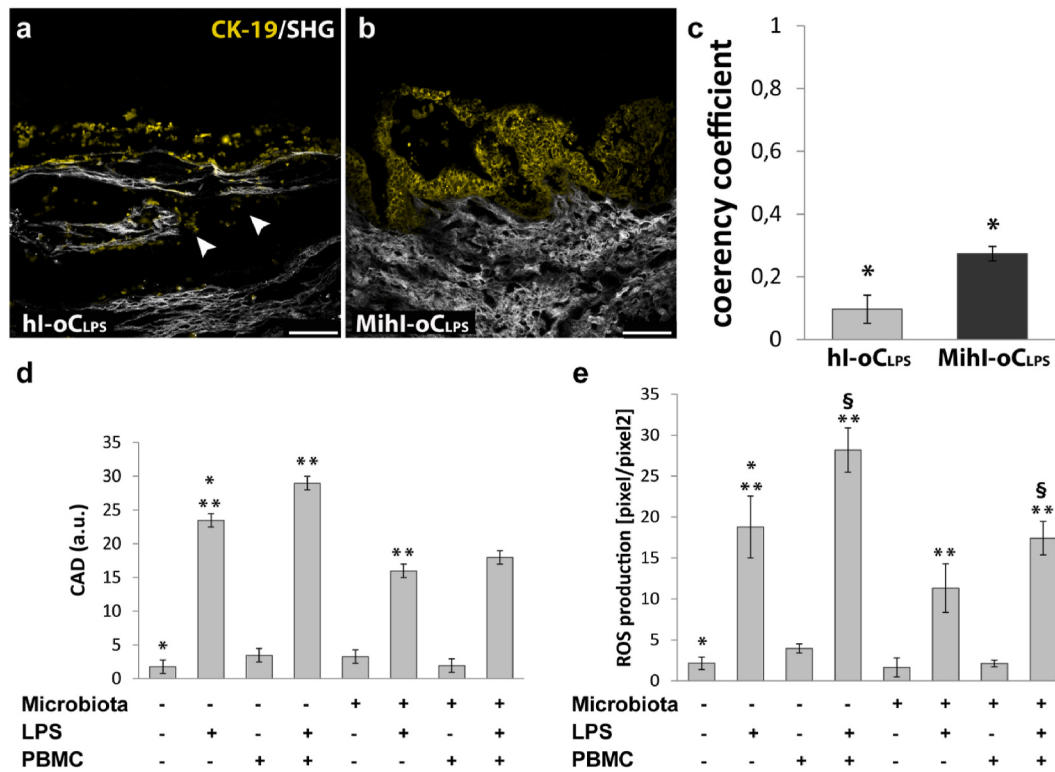


Fig. 5. Analyses of intestinal barrier dysfunction on immune-responsive Mihi-oC. Schematic representation of injured intestinal tissue model (a); histological characterization of hI-oC (b), Mihi-oC with black arrowheads indicating the microbiota (c), quantification of villi height in inflamed intestine models (hI-oC_{LPS} vs Mihi-oC_{LPS}) (d), hI-oC_{LPS} with black arrowheads that shows detached epithelial cells with spherical shape (e), Mihi-oC_{LPS} with small lesioned area as indicated by the black arrow (f), scale bar 100 μm ; high magnification H&E images indicates a luminal small area in which the bacterial translocation occurs (g), H&E image shows the blood cells recruitment to the inflammatory sites in Mihi-oC_{LPS} + PBMC (h); immunofluorescence images on 3D samples highlights the hyper-permeability at epithelial level of hI-oC_{LPS} with pixelated signal of ZO-1 (i and inset) and a network of tight junction proteins in Mihi-oC_{LPS} (j and inset), cell nuclei stained with DAPI scale bar 75 μm ; quantitative analysis of TEER values in the absence or presence of microbiota, PBMC and LPS (k), * $p < 0.001$, ** $p < 0.01$, § $p < 0.05$; quantification of ZO-1 gene expression on hI-oC_{LPS} vs Mihi-oC_{LPS} (l), * $p < 0.001$; quantitative analysis of Alcian blue-stained samples reveals the different amount of mucus production in hI-oC_{LPS} vs Mihi-oC_{LPS} (m). Data are presented as mean \pm SEM of three separate experiments, each one performed in triplicate ($n = 9$). . (For interpretation of the references to color in this figure legend, the reader is referred to the Web version of this article.)



3D scaffold, in both cases the regulatory/instructive and repository roles of the native ECM are missing. In contrast, we widely demonstrated the key role of histologically competent ECM in guiding both the epithelium morphogenesis process and in mimicking the pathophysiology of inflammation [20,22]. Here, we further increase the complexity of the intestine model, inserting on the luminal side commensal species of microbiota mainly involved in the inflammatory process and the PBMCs into the S_C to encompass the immune-competent response. Interestingly, we found an altered assembly of the collagen fibers of the hi-oC_{LPS}'s lamina propria (Fig. 7a) compared to Mihi-oC_{LPS} (Fig. 7b), highlighting a role of microbiota in exercising a defense action also on the stromal compartment of the intestine. Indeed, we investigated the level of anisotropy of collagen fibers at the sub-epithelial area by evaluating the

coherency coefficient (Fig. 7c) in SHG images. CK-19 marked road shaped epithelial cells (yellow signal) in inflamed hi-oC_{LPS} (Fig. 7a) and highlight the presence of a well polarized epithelium in Mihi-oC_{LPS} (Fig. 7b). The data of hi-oC_{LPS} indicated a high coherent orientation (coherency coefficient of 0.27 ± 0.02, isotropy condition) of the collagen fibers in a preferred direction, phenomenon already described in fibrotic and cancer microenvironment [41]. Furthermore, Fig. 7a also indicated at the stromal compartment some aligned bundles of collagen on which the epithelial cells are lined up (white arrowheads). In contrast, there was no preferential orientation of the collagen fibers in the sub-epithelial areas of the Mihi-oC_{LPS} featured by a coherency coefficient close to zero (coherency coefficient of 0.09 ± 0.04) indicating that the physiological anisotropy of collagen fibers was preserved in



these samples. Subsequently, analysis of the ECM remodeling in terms of CAD was carried out by means of Multiphoton microscopy combined with SHG imaging. In Fig. 7d, the graph indicates that the hi-oC_{LPS} was characterized by a higher amount of fibrillar collagen (27.5 ± 1.3 a. u.) compared to hi-oC samples (14.5 ± 2.1 a. u.), suggesting that the LPS induces differences in collagen microstructure organization resembling the onset of the intestinal fibrosis. Lower values of CAD were reported in MihI-oC_{LPS} (18.9 ± 2.1 a. u.) compared to hi-oC_{LPS} samples, due to the protective role exerted from the microbiota on intestinal mucosa. Slight reduction of CAD was revealed for MihI-oC samples supplemented with PBMC (14.8 ± 1.3 a. u.). Finally, MihI-oC_{LPS} supplemented with PBMC showed CAD values (16.8 ± 3.2 a. u.) comparable to an un-inflamed model (15.8 ± 3.6 a. u.). As recognized, the intestinal homeostasis is maintained by a microenvironmental redox balance [42]. It is noted that a tightly controlled ROS generation by enzymes expressed in non-phagocytic cells, for example enterocytes or fibroblasts, is a key event in the progression of many inflammatory disorders, including those involving the gastrointestinal tract [42]. In the gut inflammation, the disruption of the mucosal barrier can rapidly activate the innate immune system and set off an acute inflammatory response that begins in the lamina propria. In addition, the production of ROS by Polymorphonuclear leukocytes can create a hypoxic niche due to oxygen consumption, which may aid in the resolution of inflammation [43]. However, uncontrolled and persistent oxidative stress with over-production of ROS and/or inadequate removal of ROS by antioxidant systems will cause apoptosis and tissue injury [44,45]. Here, we investigated the oxidative stress in terms of ROS production in a hi-oC_{LPS} compared to un-inflamed one as well as the protective role exerted by the commensal microbiota in MihI-oC_{LPS}. Interestingly, a strong ROS production was estimated in hi-oC_{LPS} due to the oxidative stress induced by LPS treatment at the stromal level as reported in Fig. 6e. In our model, the crosstalk between the injured-epithelium and myofibroblasts embedded in a well-structured ECM [12,14,20] allowed us to detect the contribution of fibroblasts to ROS production even in the absence of PBMC, unlike of other models in the literature that lack of an autologous ECM [46]. In addition, the cross-talk between fibroblasts and immune cells strongly increases the ROS production in hi-oC_{LPS} + PBMC. Furthermore, even if not in direct contact, the microbiota seems to modulate the expression of cytosolic ROS at the stromal intestinal level [42]. It is known that different strains of commensal bacteria have the ability to alter the intercellular redox environment by eliciting high production of different ROS in injured epithelial barrier [47]. Surprisingly, in our model, when MihI-oC was inflamed with LPS, the cytosolic stromal ROS production was extremely reduced compared to hi-oC_{LPS} further confirming the protective role exerted by the microbiota in reducing the barrier impairment trying to restore intestinal homeostasis avoiding tissue damage (Fig. 7e and S14).

3.6. Secretome analyses in immune responsive MihI-oC

To corroborate the key role of the extracellular microenvironment at the luminal side - colonized with microbiota - and at the serosal side - flowed with PBMC - in the MihI-oC, we analyzed the pro- and anti-inflammatory cytokines profile, by collecting luminal and serosal eluates (Fig. 8a and b, S15a and b, respectively) in physiological and inflamed [48] conditions and with or without microbiota and PBMC. The different conditions allow us to analyze the contribution of multi-cellular components on the onset of inflammation. The role of the intestinal epithelial cells and fibroblasts in the induction of mucosal inflammation have been deeply investigated in the context of IBD [35]. The intestinal epithelial cells are relevant sources of pro-inflammatory and regulatory mediators, acting as modulators of the mucosal immune response by recruiting immune cells via chemokines and growth factors or regulating microbial composition [1,35,49,50]. Intestinal myofibroblasts, other than to be responsible for the production of the ECM, are also active key players of the immune system, triggered by

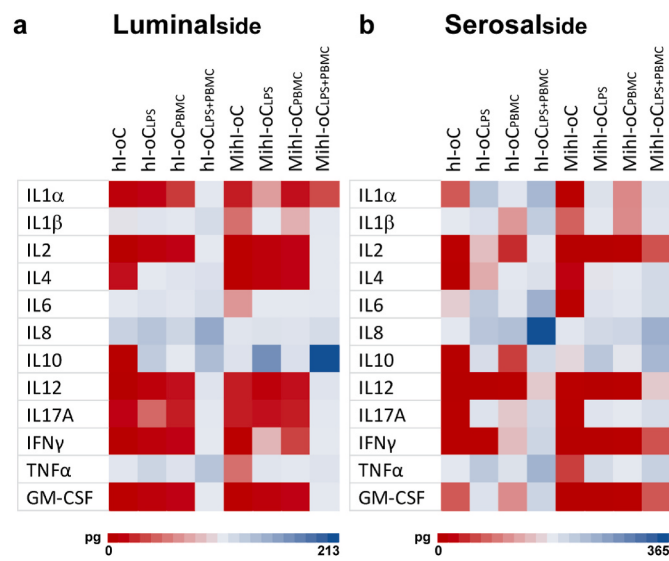


Fig. 8. Comparison of secreted immunemediators in immune responsive MihI-oC. Heatmaps indicates the secretion of inflammatory mediators collected from the luminal (a) and serosal (b) side of MihI-oC in the absence or presence of microbiota, PBMC and LPS. Data are presented as mean \pm SEM of three separate experiments, each one performed in triplicate ($n = 9$).

components of innate and adaptive immunity [51]. Myofibroblasts activation is associated with tissue injury and inflammation not only by the creation of an inflammatory environment that can promote irreversible damage of the affected tissue with fibrosis and cell proliferation in the sub-mucosa, but also by secreting a number of soluble cytokines, chemokines, growth factors, collagen, metalloproteinases, and it's inhibitors, that attract other cells to perpetuate the inflammation [52]. Recently the role of the probiotic strains in the modulation of the inflammatory response has been reported in the literature [53]. Lactobacilli and Bifidobacteria are well known to be beneficial probiotics that exert a trophic effect on the intestinal mucosa, increasing mucus production and enhancing barrier integrity [39]. Moreover, some strains modulate the expression of pro-inflammatory molecules and exert anti-inflammatory properties in a different manner compared to cells derived from peripheral blood [54,55]. Amazingly, in our model, we found high levels of the anti-inflammatory cytokine IL-10 both at the luminal and serosal levels in MihI-oC_{LPS} + PBMC, confirming the microbiota immunomodulation and immunotolerance activity, that *in vivo* is able to prevent certain IBD caused by abnormal inflammatory responses [56]. As previously reported, LPS elicited a relevant IL-8 protein expression in the supernatants collected from the luminal side of the hi-oC [12,37]. Here, the presence of microbiota quite quenched the level of released IL-8 at the luminal side while the presence of PBMC is influential on the IL-8 released at the serosal side reaching very high value when the microbiota is not present (hi-oC_{LPS} + PBMC vs MihI-oC_{LPS} + PBMC). In addition, we found that the presence of microbiota influenced the TNF- α and IL1- α release at luminal side and IL1- α , IL-2, IFN- γ and GM-CSF at serosal side in MihI-oC_{LPS} + PBMC. We argue that the commensal microbiota co-culture in MihI-oC_{LPS} + PBMC attenuates the inflammatory stimulus counteracting the damage to the intestinal barrier and trying to restore the state of homeostasis, reducing the perpetuation of inflammation. According to literature [57,58], the presence of PBMC, influences the cytokines release at serosal side, specifically IL-4 and IL-17a increases, regardless the presence of microbiota, while the increase of IL1- α and IFN- γ is quenched by the presence of microbiota (hi-oC_{PBMC} vs MihI-oC_{PBMC}). IL1- β release is also affected by the presence of PBMC, that induce its decrease (hi-oC_{PBMC} vs MihI-oC_{PBMC}), but in presence of microbiota it is not detected at all. Furthermore, low but significant levels of GM-CSF were detected at the

S_C in hI-oC_{LPS} without PBMC indicating the contribution of fibroblasts in immune cells recruitment [59]. Similar to the TEER data, the presence of microbiota *per se*, without LPS or PBMS, positively influences the cytokine profile, implying a protective effect of the probiotics against LPS-induced damage. Taken together these data indicate the multicellular contribution in the modulation of inflammation in the complex microenvironment of Mihi-oC and confirm the protective role of the microbiota on the barrier function. We found that Mihi-oC represents a relevant *in vitro* context to investigate the complex functional correlations existing among epithelial cells, stromal cells, immune cells and gut microorganism and to elucidate their role in human disease.

4. Conclusion

The immune-competent gut-microbiota axis proposed in this work is able to reproduce the architecture and vertical typography of the microbiota with a complex extracellular microenvironment consisting of a responsive ECM and a plethora of immunomodulatory mediators released from different cell populations such as epithelial, stromal, blood and microbial species in homeostatic and non-homeostatic conditions. This system is able to unbundle the single contribution of each cell and its involvement in the innate and cell-mediated inflammatory response in the onset of the inflammation process. Mihi-oC provides a useful platform for inflammation studies such as ileitis, IBD or diseases (Crohn's disease or zonulin-mediated gut disease). By implementing the M_C , Mihi-oC favors the cultivation of the various microbial species of the intestinal microbiota (microaerophilic and anaerobic) allowing the vertical stratification of the bacteria species. Furthermore, Mihi-oC could be used for future studies of drug testing or active food digestion and could be implemented with other modules that mimic different organs such as the blood brain barrier by reconstructing a microbiota Gut-brain axis, adipose tissue for obesity studies or with the liver to evaluate drug toxicity.

Credit author statement

Vincenza De Gregorio: Conceptualization, Methodology, Software, Validation, Formal analysis, Investigation, Data curation, Writing.
Cinzia Sgambato: Investigation, Methodology, Formal analysis.
Vincenza De Gregorio, Francesco Urciuolo, Raffaele Vecchione: Writing – review & editing.
Giorgia Imparato, Paolo Antonio Netti: Writing – review & editing.
Giorgia Imparato: Conceptualization, Writing – review & editing, Supervision.

Data availability

The raw/processed data required to reproduce these findings cannot be shared at this time due to technical or time limitations.

Declaration of competing interest

The authors declare that they have no known competing financial interests or personal relationships that could have appeared to influence the work reported in this paper.

Acknowledgments

The authors would like to thank Dr. Alessia La Rocca for kindly providing the images of schematic representation of small intestine and Dr. Brunella Corrado for CAD of Mihi-oC components. The authors declare that they have no competing interests.

Appendix A. Supplementary data

Supplementary data to this article can be found online at <https://doi.org/10.1016/j.biomaterials.2022.121573>.

References

- [1] Y. Belkaid, T.W. Hand, Role of the microbiota in immunity and inflammation, *Cell* 157 (1) (2014) 121–141.
- [2] G.M. Douglas, R. Hansen, C.M.A. Jones, K.A. Dunn, A.M. Comeau, J.P. Bielawski, R. Tayler, E.M. El-Omar, R.K. Russell, G.L. Hold, M.G.I. Langille, J. Van Limbergen, Multi-omics differentially classify disease state and treatment outcome in pediatric Crohn's disease, *Microbiome* 6 (1) (2018) 13.
- [3] N. Arumugasaamy, J. Navarro, J. Kent Leach, P.C.W. Kim, J.P. Fisher, In vitro models for studying transport across epithelial tissue barriers, *Ann. Biomed. Eng.* 47 (1) (2019) 1–21.
- [4] G.P. Donaldson, S.M. Lee, S.K. Mazmanian, Gut biogeography of the bacterial microbiota, *Nat. Rev. Microbiol.* 14 (1) (2016) 20–32.
- [5] C. Gusils, V. Morata, S. Gonzalez, Determination of bacterial adhesion to intestinal mucus, *Methods Mol. Biol.* 268 (2004) 411–415.
- [6] F.L. Hellweger, R.J. Clegg, J.R. Clark, C.M. Plugge, J.U. Kreft, Advancing microbial sciences by individual-based modelling, *Nat. Rev. Microbiol.* 14 (7) (2016) 461–471.
- [7] M. Marzorati, B. Vanhoecke, T. De Ryck, M. Sadaghian Sadabadi, I. Pinheiro, S. Possemiers, P. Van den Abbeele, L. Derycke, M. Bracke, J. Pieters, T. Hennebel, H.J. Harmsen, W. Verstraete, T. Van de Wiele, The HMI module: a new tool to study the Host-Microbiota Interaction in the human gastrointestinal tract *in vitro*, *BMC Microbiol.* 14 (2014) 133.
- [8] P. Shah, J.V. Fritz, E. Glaab, M.S. Desai, K. Greenhalgh, A. Frachet, M. Niegowska, M. Estes, C. Jager, C. Seguin-Devaux, F. Zenhausern, P. Wilmes, A microfluidics-based *in vitro* model of the gastrointestinal human-microbe interface, *Nat. Commun.* 7 (2016) 11535.
- [9] S. Jalili-Firoozinezhad, F.S. Gazzaniga, E.L. Calamari, D.M. Camacho, C.W. Fadel, A. Bein, B. Swenor, B. Nestor, M.J. Cronce, A. Tovaglieri, O. Levy, K.E. Gregory, D.T. Breault, J.M.S. Cabral, D.L. Kaspar, R. Novak, D.E. Ingber, A complex human gut microbiome cultured in an anaerobic intestine-on-a-chip, *Nat Biomed Eng* 3 (7) (2019) 520–531.
- [10] D.C. Stewart, D. Berrie, J. Li, X. Liu, C. Rickerson, D. Mkoji, A. Iqbal, S. Tan, A. L. Doty, S.C. Glover, C.S. Simmons, Quantitative assessment of intestinal stiffness and associations with fibrosis in human inflammatory bowel disease, *PLoS One* 13 (7) (2018), e0200377.
- [11] N.J. Darling, C.L. Mobbs, A.L. Gonzalez-Hau, M. Freer, S. Przyborski, Bioengineering novel *in vitro* Co-culture models that represent the human intestinal mucosa with improved caco-2 structure and barrier function, *Front. Bioeng. Biotechnol.* 8 (2020) 992.
- [12] V. De Gregorio, G. Imparato, F. Urciuolo, P.A. Netti, Micro-patterned endogenous stroma equivalent induces polarized crypt-villus architecture of human small intestinal epithelium, *Acta Biomater.* 81 (2018) 43–59.
- [13] Y. Wang, R. Kim, S.S. Hinman, B. Zwarycz, S.T. Magness, N.L. Allbritton, Bioengineered systems and designer matrices that recapitulate the intestinal stem cell niche, *Cell Mol Gastroenterol Hepatol* 5 (3) (2018) 440–453 e1.
- [14] V. De Gregorio, G. Imparato, F. Urciuolo, P.A. Netti, 3D stromal tissue equivalent affects intestinal epithelium morphogenesis *in vitro*, *Biotechnol. Bioeng.* 115 (4) (2018) 1062–1075.
- [15] A. Garziano, F. Urciuolo, G. Imparato, F. Martorina, B. Corrado, P. Netti, A micro-perfusion bioreactor for on line investigation of ECM remodeling under hydrodynamics and biochemical stimulation, *Lab Chip* 16 (5) (2016) 855–867.
- [16] F. Urciuolo, A. Garziano, G. Imparato, V. Panzetta, S. Fusco, C. Casale, P.A. Netti, Biophysical properties of dermal building-blocks affects extra cellular matrix assembly in 3D endogenous macrotissue, *Biofabrication* 8 (1) (2016), 015010.
- [17] M. Klinger, L.P. Tolbold, K.V. Gothelf, P.R. Ogilby, Effect of polymer cross-links on oxygen diffusion in glassy PMMA films, *ACS Appl. Mater. Interfaces* 1 (3) (2009) 661–667.
- [18] R.H. Lam, M.C. Kim, T. Thorsen, Culturing aerobic and anaerobic bacteria and mammalian cells with a microfluidic differential oxygenator, *Anal. Chem.* 81 (14) (2009) 5918–5924.
- [19] G. Donnarumma, A. Molinaro, D. Cimini, C. De Castro, V. Valli, V. De Gregorio, M. De Rosa, C. Schiraldi, Lactobacillus crispatus L1: high cell density cultivation and exopolysaccharide structure characterization to highlight potentially beneficial effects against vaginal pathogens, *BMC Microbiol.* 14 (2014) 137.
- [20] V. De Gregorio, B. Corrado, S. Sbrescia, S. Sibilio, F. Urciuolo, P.A. Netti, G. Imparato, Intestine-on-chip device increases ECM remodeling inducing faster epithelial cell differentiation, *Biotechnol. Bioeng.* 117 (2) (2020) 556–566.
- [21] E. Fonck, G.G. Feigl, J. Fasel, D. Sage, M. Unser, D.A. Rufenacht, N. Stergiopoulos, Effect of aging on elastin functionality in human cerebral arteries, *Stroke* 40 (7) (2009) 2552–2556.
- [22] V. De Gregorio, M. Telesco, B. Corrado, V. Rosiello, F. Urciuolo, P.A. Netti, G. Imparato, Intestine-liver Axis on-chip reveals the intestinal protective role on hepatic damage by emulating ethanol first-pass metabolism, *Front. Bioeng. Biotechnol.* 8 (2020) 163.
- [23] Y. Xiang, H. Wen, Y. Yu, M. Li, X. Fu, S. Huang, Gut-on-chip: recreating human intestine *in vitro*, *J. Tissue Eng.* 11 (2020), 2041731420965318.
- [24] S.N. Bhatia, D.E. Ingber, Microfluidic organs-on-chips, *Nat. Biotechnol.* 32 (8) (2014) 760–772.
- [25] S. Muenchau, R. Deutsch, I.J. de Castro, T. Hielscher, N. Heber, B. Niesler, M. Lusic, M.L. Stanifer, S. Boulant, Hypoxic environment promotes barrier formation in human intestinal epithelial cells through regulation of MicroRNA 320a expression, *Mol. Cell Biol.* 39 (14) (2019).
- [26] L. Zheng, C.J. Kelly, S.P. Colgan, Physiologic hypoxia and oxygen homeostasis in the healthy intestine. A review in the theme: cellular responses to hypoxia, *Am. J. Physiol. Cell Physiol.* 309 (6) (2015) C350–C360.

- [27] N.E. Zeitouni, S. Chotikatum, M. von Kockritz-Blickwede, H.Y. Naim, The impact of hypoxia on intestinal epithelial cell functions: consequences for invasion by bacterial pathogens, *Mol Cell Pediatr* 3 (1) (2016) 14.
- [28] M.G. Espy, Role of oxygen gradients in shaping redox relationships between the human intestine and its microbiota, *Free Radic. Biol. Med.* 55 (2013) 130–140.
- [29] S. Kawasaki, M. Nagasaku, T. Mimura, H. Katashima, S. Ijuuin, T. Satoh, Y. Niimura, Effect of CO₂ on colony development by *Bifidobacterium* species, *Appl. Environ. Microbiol.* 73 (23) (2007) 7796–7798.
- [30] K. Ninomiya, K. Matsuda, T. Kawahata, T. Kanaya, M. Kohno, Y. Katakura, M. Asada, S. Shioya, Effect of CO₂ concentration on the growth and exopolysaccharide production of *Bifidobacterium longum* cultivated under anaerobic conditions, *J. Biosci. Bioeng.* 107 (5) (2009) 535–537.
- [31] W. Shin, A. Wu, M.W. Massidda, C. Foster, N. Thomas, D.W. Lee, H. Koh, Y. Ju, J. Kim, H.J. Kim, A robust longitudinal Co-culture of obligate anaerobic gut microbiome with human intestinal epithelium in an anoxic-oxic interface-on-a-chip, *Front. Bioeng. Biotechnol.* 7 (2019) 13.
- [32] E. Martini, S.M. Krug, B. Siegmund, M.F. Neurath, C. Becker, Mend your fences: the epithelial barrier and its relationship with mucosal immunity in inflammatory bowel disease, *Cell Mol Gastroenterol Hepatol* 4 (1) (2017) 33–46.
- [33] M. Herath, S. Hosie, J.C. Bornstein, A.E. Franks, E.L. Hill-Yardin, The role of the gastrointestinal mucus system in intestinal homeostasis: implications for neurological disorders, *Front. Cell. Infect. Microbiol.* 10 (2020) 248.
- [34] I. von Ossowski, J. Reunanan, R. Satokari, S. Vesterlund, M. Kankainen, H. Huhtinen, S. Tynkkynen, S. Salminen, W.M. de Vos, A. Palva, Mucosal adhesion properties of the probiotic *Lactobacillus rhamnosus* GG SpaCBA and SpaFED pilin subunits, *Appl. Environ. Microbiol.* 76 (7) (2010) 2049–2057.
- [35] R. Curciarello, K.E. Canziani, G.H. Docena, C.I. Muglia, Contribution of non-immune cells to activation and modulation of the intestinal inflammation, *Front. Immunol.* 10 (2019) 647.
- [36] M. Maurer, M.S. Gresnigt, A. Last, T. Wollny, F. Berlinghof, R. Pospich, Z. Cseresnyes, A. Medyukhina, K. Graf, M. Groger, M. Raasch, F. Siwcak, S. Nietzsche, I.D. Jacobsen, M.T. Figge, B. Hube, O. Huber, A.S. Mosig, A three-dimensional immunocompetent intestine-on-chip model as in vitro platform for functional and microbial interaction studies, *Biomaterials* 220 (2019) 119396.
- [37] H.J. Kim, H. Li, J.J. Collins, D.E. Ingber, Contributions of microbiome and mechanical deformation to intestinal bacterial overgrowth and inflammation in a human gut-on-a-chip, *Proc. Natl. Acad. Sci. U. S. A.* 113 (1) (2016) E7–E15.
- [38] A. Habtezion, L.P. Nguyen, H. Hadeiba, E.C. Butcher, Leukocyte trafficking to the small intestine and colon, *Gastroenterology* 150 (2) (2016) 340–354.
- [39] P. Hemarajata, J. Versalovic, Effects of probiotics on gut microbiota: mechanisms of intestinal immunomodulation and neuromodulation, *Therap Adv Gastroenterol* 6 (1) (2013) 39–51.
- [40] C.A. Alemao, K.F. Budden, H.M. Gomez, S.F. Rehman, J.E. Marshall, S.D. Shukla, C. Donovan, S.C. Forster, I.A. Yang, S. Keely, E.R. Mann, E.M. El Omar, G.T. Belz, P. M. Hansbro, Impact of diet and the bacterial microbiome on the mucous barrier and immune disorders, *Allergy* 76 (3) (2021) 714–734.
- [41] S.Z. Despotovic, D.N. Milicevic, A.J. Krmpot, A.M. Pavlovic, V.D. Zivanovic, Z. Krivokapic, V.B. Pavlovic, S. Levic, G. Nikolic, M.D. Rabasovic, Altered organization of collagen fibers in the uninvolved human colon mucosa 10 cm and 20 cm away from the malignant tumor, *Sci. Rep.* 10 (1) (2020) 6359.
- [42] G. Aviello, U.G. Knaus, ROS in gastrointestinal inflammation: rescue or Sabotage? *Br. J. Pharmacol.* 174 (12) (2017) 1704–1718.
- [43] E.L. Campbell, W.J. Bruyninx, C.J. Kelly, L.E. Glover, E.N. McNamee, B. E. Bowers, A.J. Bayless, M. Scully, B.J. Saeedi, L. Golden-Mason, S.F. Ehrentraut, V. F. Curtis, A. Burgess, J.F. Garvey, A. Sorensen, R. Nemenoff, P. Jedlicka, C. T. Taylor, D.J. Kominsky, S.P. Colgan, Transmigrating neutrophils shape the mucosal microenvironment through localized oxygen depletion to influence resolution of inflammation, *Immunity* 40 (1) (2014) 66–77.
- [44] M.H. Raza, K. Gul, A. Arshad, N. Riaz, U. Waheed, A. Rauf, F. Aldakheel, S. Alduraywish, M.U. Rehman, M. Abdullah, M. Arshad, Microbiota in cancer development and treatment, *J. Cancer Res. Clin. Oncol.* 145 (1) (2019) 49–63.
- [45] A. Rezaie, R.D. Parker, M. Abdollahi, Oxidative stress and pathogenesis of inflammatory bowel disease: an epiphomenon or the cause? *Dig. Dis. Sci.* 52 (9) (2007) 2015–2021.
- [46] W. Shin, H.J. Kim, Intestinal barrier dysfunction orchestrates the onset of inflammatory host-microbiome cross-talk in a human gut inflammation-on-a-chip, *Proc. Natl. Acad. Sci. U. S. A.* 115 (45) (2018), E10539–E10547.
- [47] R.M. Jones, J.W. Mercante, A.S. Neish, Reactive oxygen production induced by the gut microbiota: pharmacotherapeutic implications, *Curr. Med. Chem.* 19 (10) (2012) 1519–1529.
- [48] F.A. Omonijo, S. Liu, Q. Hui, H. Zhang, L. Lahaye, J.C. Bodin, J. Gong, M. Nyachoti, C. Yang, Thymol improves barrier function and attenuates inflammatory responses in porcine intestinal epithelial cells during lipopolysaccharide (LPS)-Induced inflammation, *J. Agric. Food Chem.* 67 (2) (2019) 615–624.
- [49] C. Andrews, M.H. McLean, S.K. Durum, Cytokine tuning of intestinal epithelial function, *Front. Immunol.* 9 (2018) 1270.
- [50] M. Sichetti, S. De Marco, R. Pagioti, G. Traina, D. Pietrella, Anti-inflammatory effect of multistrain probiotic formulation (*L. rhamnosus*, *B. lactis*, and *B. longum*), *Nutrition* 53 (2018) 95–102.
- [51] C. Bonnans, J. Chou, Z. Werb, Remodelling the extracellular matrix in development and disease, *Nat. Rev. Mol. Cell Biol.* 15 (12) (2014) 786–801.
- [52] D.W. Powell, R.C. Mifflin, J.D. Valentich, S.E. Crowe, J.I. Saada, A.B. West, Myofibroblasts. I. Paracrine cells important in health and disease, *Am. J. Physiol.* 277 (1) (1999) C1–C9.
- [53] F. Cristofori, V.N. Dargenio, C. Dargenio, V.L. Miniello, M. Barone, R. Francavilla, Anti-inflammatory and immunomodulatory effects of probiotics in gut inflammation: a door to the body, *Front. Immunol.* 12 (2021) 578386.
- [54] R.S. Longman, Y. Yang, G.E. Diehl, S.V. Kim, D.R. Littman, Microbiota: host interactions in mucosal homeostasis and systemic autoimmunity, *Cold Spring Harb Symp Quant Biol* 78 (2013) 193–201.
- [55] M.A.K. Azad, M. Sarker, D. Wan, Immunomodulatory effects of probiotics on cytokine profiles, *BioMed Res. Int.* 2018 (2018) 8063647.
- [56] A. de Moreno de Leblanc, S. Del Carmen, M. Zurita-Turk, C. Santos Rocha, M. van de Guchte, V. Azevedo, A. Miyoshi, J.G. Leblanc, Importance of IL-10 modulation by probiotic microorganisms in gastrointestinal inflammatory diseases, *ISRN Gastroenterol* 2011 (2011) 892971.
- [57] C.A. Dinarello, Overview of the IL-1 family in innate inflammation and acquired immunity, *Immunol. Rev.* 281 (1) (2018) 8–27.
- [58] W. Jin, C. Dong, IL-17 cytokines in immunity and inflammation, *Emerg Microbes Infect* 2 (9) (2013) e60.
- [59] J. Dabritz, Granulocyte macrophage colony-stimulating factor and the intestinal innate immune cell homeostasis in Crohn's disease, *Am. J. Physiol. Gastrointest. Liver Physiol.* 306 (6) (2014) G455–G465.

Appendix: Abbreviation

Caco-2: Human colonic epithelial cell lines
hISEMFs: human intestinal subepithelial myofibroblasts
PBMC: Human peripheral blood mononuclear cells
L rhamnosus: *Lactobacillus rhamnosus*
B longum: *Bifidobacterium longum*
3D-hI: three-dimensional human intestine model
I_C: Intestine compartment
S_C: serosal compartment
PDMS: polydimethylsiloxane
PMMA: poly(methyl methacrylate)
hI-oC: human intestine on a chip
MihI-oC: Microbiota human Intestine on a chip
M_C: Microbiota chamber
AW: anaerobic workstation
micro-AW: microaerophilic conditions in the Anaerobic Workstation
ana-AW: anaerobic conditions in the Anaerobic Workstation
LPS: lipopolysaccharides from *Escherichia coli*
hI-oC_{LPS}: Inflamed human intestine on-chip
MihI-oC_{LPS}: Inflamed Microbiota human Intestine on chip
hI-oC_{PBMC}: Immune-responsive human intestine on chip
MihI-oC_{PBMC}: Immune-responsive Microbiota human Intestine on chip
hI-oC_{LPS} + PBMC: Inflamed Immune-responsive human intestine on chip
MihI-oC_{LPS} + PBMC: Inflamed Immune-responsive Microbiota human Intestine on chip
CAD: collagen assembly degree